PHILOSOPHICAL TRANSACTIONS OF THE ROYAL SOCIETY A MATHEMATICAL, PHYSICAL & ENGINEERING SCIENCES

Integrable and Chaotic Motions of Four Vortices II. Collision Dynamics of Vortex Pairs

B. Eckhardt and H. Aref

Phil. Trans. R. Soc. Lond. A 1988 **326**, 655-696
doi: 10.1098/rsta.1988.0117

Phil. Trans. R. Soc. Lond. A **326**, 655–696 (1988) [655]
Printed in Great Britain

INTEGRABLE AND CHAOTIC MOTIONS OF FOUR VORTICES
II. COLLISION DYNAMICS OF VORTEX PAIRS

By B. Eckhardt[1]† and H. Aref[2]

[1] *FB Physik, Universität Bremen*, 2800 *Bremen* 33, *F.R.G.*

[2] *Institute of Geophysics and Planetary Physics and Department of Applied Mechanics and Engineering Science, University of California, San Diego, La Jolla, California* 92093, *U.S.A.*

(*Communicated by J. T. Stuart, F.R.S. – Received* 24 *July* 1987)

CONTENTS

The interaction of two vortex pairs is investigated analytically and by numerical experiments from the vantage point of dynamical-systems theory. Vortex pairs can escape to infinity, so the phase space of this system is unbounded in contrast to that of four identical vortices investigated previously. Chaotic motion is nevertheless possible both for 'bound states' of the system and for 'scattering states'. For the bound states standard Poincaré section techniques suffice. For scattering states chaos appears as complex structure in the numerically generated plot of scattering angle against impact parameter. Interpretations of physical space mechanisms leading to chaos are given. Analytical characterizations of the system include a formal reduction to two degrees of freedom by canonical transformations and an identification and discussion of integrable cases of which one is apparently new.

† Present address: Institut für Festkörperforschung, Kernforschungsanlage, 5170 Jülich, F.R.G.

1. Introduction

In the first part of this study (Aref & Pomphrey 1982†; henceforth referred to as part 1) chaotic behaviour in the dynamics of four identical vortices was demonstrated and analysed. In this paper we consider the case where the vortex strengths satisfy $\kappa_1 = -\kappa_4, \kappa_2 = -\kappa_3$. The most important difference from the system studied in part 1 is the possibility of unbounded motion. Neutral vortex pairs, such as vortices 1 and 4 (or 2 and 3) can propagate to infinity. We are again primarily interested in identifying and studying those portions of phase space where chaotic motion is to be found.

The paper proceeds much as part 1 (and the notation is largely consistent with that used there). In §2 we show how a point vortex system with n neutral pairs, and thus $N = 2n$ degrees of freedom, can be reduced to a hamiltonian system with $N-2$ degrees of freedom by canonical transformations. A similar result was achieved for identical vortices in part 1. Related work has been published by Khanin (1982).

In §3 the formalism is applied to a single pair for illustrative purposes. Application to the case $N = 4$ follows, and §3 concludes with a discussion of certain special solutions for two-pair motion. Some of these solutions have been known for at least a century. Additional details of integrable cases are collected in Appendixes A and B.

In §4 we report numerical experiments identifying regions of phase space where chaotic behaviour is of importance. Here we extend previous studies by Manakov & Shchur (1983).

The concluding §5 contains a discussion of our results, in particular their relation to other investigations of chaotic behaviour in problems with scattering states, and their significance for two-dimensional hydrodynamics.

For a brief introduction to this paper see the letter by Eckhardt (1988*a*).

2. Reduction of degrees of freedom by canonical transformations

As discussed in part 1 and in several places in the literature (Kirchhoff 1876; Lamb 1932; Batchelor 1967, chap. 7) the dynamics of N point vortices defines a hamiltonian system. In the following analysis N is assumed even, $N = 2n$, and the vortex positions in the flow plane are designated by complex numbers, $z_l^{(s)}$, where $l = 1, \ldots, n$ and $s = \pm$. The vortices at $z_l^{(+)}, z_l^{(-)}$ have circulations or strengths $+\kappa_l$ and $-\kappa_l$, respectively (where we assume $\kappa_l > 0$).

The fundamental Poisson brackets (see part 1, §2) are

$$[z_l^{(s)}, z_m^{(s')}] = 0, \quad [z_l^{(s)}, z_m^{(s')*}] = -2\mathrm{i}s\delta_{ss'}\delta_{lm}/\kappa_l, \tag{2.1 a, b}$$

where $l, m = 1, \ldots, n$; $s, s' = \pm$. We now introduce the variables

$$\sigma_l^{(+)} = \tfrac{1}{2}(z_l^{(+)} + z_l^{(-)}), \quad \sigma_l^{(-)} = \kappa_l(z_l^{(+)} - z_l^{(-)}), \tag{2.2 a, b}$$

for $l = 1, \ldots, n$. Clearly $\sigma_l^{(+)}$ gives the location of the midpoint of the line joining the vortices in

† On p. 377 and in the caption of figure 8 in that paper the quantity A_c appears as $(2\sqrt{3})/3$. This is a misprint. The correct value is $A_c = 2/(3\sqrt{3})$.

the lth pair (positions $z_l^{(+)}$ and $z_l^{(-)}$), whereas $\sigma_l^{(-)}$ is the impulse carried by that pair. The quantities $\sigma_l^{(s)}$ satisfy the Poisson bracket relations

$$[\sigma_l^{(s)}, \sigma_m^{(s')}] = 0, \quad [\sigma_l^{(s)}, \sigma_m^{(s')*}] = -2\mathrm{i}\delta_{s,-s'}\delta_{l,m}. \tag{2.3a,b}$$

The formulae

$$z_l^{(s)} = \sigma_l^{(+)} + (s/2\kappa_l)\,\sigma_l^{(-)} \tag{2.4}$$

express the vortex coordinates in terms of the $\sigma_l^{(s)}$.

It is straightforward to calculate the integrals of motion $\sum \kappa_\alpha z_\alpha$ and $\sum \kappa_\alpha |z_\alpha|^2$ in terms of the $\sigma_l^{(s)}$. One obtains

$$Q + \mathrm{i}P \equiv \sum_{\alpha=1}^{N} \kappa_\alpha z_\alpha = \sum_{l=1}^{n} \sigma_l^{(-)} \tag{2.5}$$

and

$$I \equiv \sum_{\alpha=1}^{N} \kappa_\alpha |z_\alpha|^2 = 2\sum_{l=1}^{n} \mathrm{Re}\,(\sigma_l^{(+)*}\,\sigma_l^{(-)}). \tag{2.6}$$

(In part 1 this quantity was always positive and was, thus, called L^2.)

To produce canonical variables we let

$$\sigma_l^{(s)} = q_l^{(s)} + \mathrm{i}p_l^{(-s)}, \tag{2.7}$$

where $q_l^{(s)}, p_l^{(s)}$ are real. It is then easy to see that (2.3) implies

$$[q_l^{(s)}, q_m^{(s')}] = [p_l^{(s)}, p_m^{(s')}] = 0, \quad [q_l^{(s)}, p_m^{(s')}] = \delta_{s,s'}\delta_{l,m}, \tag{2.8a,b}$$

so that $q_l^{(s)}, p_l^{(s)}$ are indeed canonical variables for $l = 1, \ldots, n$; $s = \pm$. In terms of these new variables, (2.5) and (2.6) become

$$Q + \mathrm{i}P = \sum_{l=1}^{n} q_l^{(-)} + \mathrm{i}p_l^{(+)}, \tag{2.9}$$

$$I = 2\sum_{l=1}^{n} q_l^{(+)} q_l^{(-)} + p_l^{(+)} p_l^{(-)}. \tag{2.10}$$

Equation (2.9) then suggests introducing another set of real variables $Q_\mu^{(s)}, P_\mu^{(s)}$ through

$$Q_\mu^{(s)} + \mathrm{i}P_\mu^{(-s)} = n^{-\frac{1}{2}} \sum_{l=1}^{n} (q_l^{(s)} + \mathrm{i}p_l^{(-s)})\, \mathrm{e}^{\mathrm{i}2\pi\mu(l-1)/n}, \tag{2.11}$$

where $\mu = 0, 1, \ldots, n-1$ and $s = \pm$. Note that (2.11) represents a discrete Fourier transform of the $\sigma_l^{(s)}$ thought of as an array of complex data. This development is quite analogous to that of part 1. The essential new step is the introduction of the 'pair variables' $\sigma_l^{(s)}$ in (2.2).

It follows from (2.10) and (2.11) that

$$I = 2\sum_{\mu=0}^{n-1} Q_\mu^{(+)} Q_\mu^{(-)} + P_\mu^{(+)} P_\mu^{(-)} \tag{2.12}$$

a result that we shall need in §3*b*. It also follows (see part 1, §3) that $Q_\mu^{(s)}$ and $P_\mu^{(s)}$ are canonically conjugate for all $\mu = 0, 1, \ldots, n-1$ and $s = \pm$. Finally it is clear from (2.9) that

$$Q + \mathrm{i}P = (Q_0^{(-)} + \mathrm{i}P_0^{(+)})\sqrt{n}. \tag{2.13}$$

Thus $Q_0^{(-)}$ and $P_0^{(+)}$ are integrals of the motion and their conjugate variables, $P_0^{(-)}$ and $Q_0^{(+)}$ respectively, are cyclic. The hamiltonian written in terms of the $Q_\mu^{(s)}, P_\mu^{(s)}$ therefore can be thought of as describing a system with only $N-2$ degrees of freedom ($\mu = 1, \ldots, n-1$; $s = \pm$).

PHILOSOPHICAL TRANSACTIONS OF THE ROYAL SOCIETY A MATHEMATICAL, PHYSICAL & ENGINEERING SCIENCES

The quantities $Q_0^{(-)}, P_0^{(+)}$, which according to (2.13) are just the components of the fluid impulse, or because the total circulation vanishes the fluid momentum (see Lamb 1932, chap. 7; Batchelor 1967, chap. 7) appear as parameters. The variables $Q_0^{(+)}, P_0^{(-)}$ are absent from the hamiltonian. Their evolution must be determined subsequently by solving

$$\dot{Q}_0^{(+)} = \partial H/\partial P_0^{(+)}, \quad \dot{P}_0^{(-)} = -\partial H/\partial Q_0^{(-)}, \tag{2.14a,b}$$

where H is the hamiltonian (which will be given explicitly in §3).

In summary, a reduction of degrees of freedom from N to $N-2$ has been accomplished.

3. The reduced hamiltonian

In general the hamiltonian for N point vortices with strengths κ_α and positions z_α, $\alpha = 1, \ldots, N$, is (see part 1, §2)

$$H = -(2\pi)^{-1} \sum_{1 \leqslant \alpha < \beta \leqslant N} \kappa_\alpha \kappa_\beta \ln |z_\alpha - z_\beta|. \tag{3.1}$$

Labelling the vortices according to l and s as in §2 we obtain

$$H = (2\pi)^{-1} \left\{ \sum_{l=1}^{n} \kappa_l^2 \ln |z_l^{(+)} - z_l^{(-)}| - \sum_{1 \leqslant l < m \leqslant n} \kappa_l \kappa_m \sum_{s,s' = \pm} ss' \ln |z_l^{(s)} - z_m^{(s')}| \right\}. \tag{3.2}$$

To write H in terms of the $Q_\mu^{(s)}, P_\mu^{(s)}$ of §2 we must invert (2.11), i.e.

$$z_l^{(s)} = n^{-\frac{1}{2}} \sum_{\mu=0}^{n-1} \mathrm{e}^{-\mathrm{i}2\pi\mu(l-1)/n} \{ Q_\mu^{(+)} + \mathrm{i}P_\mu^{(-)} + (s/2\kappa_l)\,(Q_\mu^{(-)} + \mathrm{i}P_\mu^{(+)}) \}. \tag{3.3}$$

Combining (3.3) with (3.2) yields the desired result. We now turn to special cases.

(a) *The case $N = 2$: a single pair*

This is trivial but, nevertheless, illustrative. Equation (3.3) becomes

$$z_+ = \{ Q_+ + \mathrm{i}P_- + (Q_- + \mathrm{i}P_+)/2\kappa \}, \quad z_- = \{ Q_+ + \mathrm{i}P_- - (Q_- + \mathrm{i}P_+)/2\kappa \}, \tag{3.4a,b}$$

where we have adopted the obvious abbreviations $z_s = z_1^{(s)}$, $Q_s = Q_0^{(s)}$, $P_s = P_0^{(s)}$, $s = \pm$ and $\kappa = \kappa_1$. Thus,

$$z_+ - z_- = (Q_- + \mathrm{i}P_+)/\kappa \tag{3.4c}$$

and the hamiltonian is

$$H_1 = (\kappa^2/4\pi) \ln (Q_-^2 + P_+^2). \tag{3.5}$$

Note that Q_- and P_+ are integrals of the motion.

The equations of motion for Q_+ and P_-, (2.14), become

$$\dot{Q}_+ = \partial H_1/\partial P_+ = (\kappa^2/2\pi)\, P_+/(Q_-^2 + P_+^2), \tag{3.6a}$$

$$\dot{P}_- = -\partial H_1/\partial Q_- = -(\kappa^2/2\pi)\, Q_-/(Q_-^2 + P_+^2). \tag{3.6b}$$

From (3.4c) we see that $Q_-^2 + P_+^2 = \kappa^2 d^2$, where d is the (constant) separation of the pair. It follows that

$$Q_+(t) = Q_+(0) + P_+ t/2\pi d^2, \quad P_-(t) = P_-(0) - Q_- t/2\pi d^2, \tag{3.7a,b}$$

whence

$$z_s(t) = z_s(0) + (P_+ - \mathrm{i}Q_-)\, t/2\pi d^2 \tag{3.8a}$$

or

$$z_s(t) = z_s(0) - \mathrm{i}\kappa(z_+ - z_-)\, t/2\pi d^2. \tag{3.8b}$$

This is, of course, the standard result of uniform linear translation.

(*b*) *The case* $N = 4$*: two vortex pairs*

We begin by writing out the transformation equations (2.11) and their inverses, (3.3). It is convenient to introduce the abbreviations

$$\Gamma \equiv \sqrt{(\kappa_1 \kappa_2)}; \quad \lambda = \sqrt{(\kappa_1/\kappa_2)}. \tag{3.9a}$$

Then

$$\kappa_1 = \lambda\Gamma; \quad \kappa_2 = \lambda^{-1}\Gamma. \tag{3.9b}$$

We also introduce the abbreviations $\zeta_0, \hat{\zeta}_0, \zeta_\pm$ via (2.11) as follows†:

$$\zeta_0 \equiv (Q_0^{(-)} + iP_0^{(+)})/\sqrt{2} = \tfrac{1}{2}\Gamma(\lambda(z_1^{(+)} - z_1^{(-)}) + \lambda^{-1}(z_2^{(+)} - z_2^{(-)})\}, \tag{3.10a}$$

$$\hat{\zeta}_0 \equiv (Q_0^{(+)} + iP_0^{(-)})\sqrt{2} = \tfrac{1}{2}(z_1^{(+)} + z_1^{(-)} + z_2^{(+)} + z_2^{(-)}, \tag{3.10b}$$

$$\zeta_+ \equiv (Q_1^{(+)} + iP_1^{(-)})\sqrt{2} = \tfrac{1}{2}(z_1^{(+)} + z_1^{(-)} - z_2^{(+)} - z_2^{(-)}), \tag{3.10c}$$

$$\zeta_- \equiv (Q_1^{(-)} + iP_1^{(+)})/\sqrt{2} = \tfrac{1}{2}\Gamma\{\lambda(z_1^{(+)} - z_1^{(-)}) - \lambda^{-1}(z_2^{(+)} - z_2^{(-)})\}. \tag{3.10d}$$

The inverse transformation is

$$z_1^{(+)} = \tfrac{1}{2}\{\hat{\zeta}_0 + \zeta_+ + (\zeta_0 + \zeta_-)/\lambda\Gamma\}, \tag{3.11a}$$

$$z_1^{(-)} = \tfrac{1}{2}\{\hat{\zeta}_0 + \zeta_+ - (\zeta_0 + \zeta_-)/\lambda\Gamma\}, \tag{3.11b}$$

$$z_2^{(+)} = \tfrac{1}{2}\{\hat{\zeta}_0 - \zeta_+ + \lambda(\zeta_0 - \zeta_-)/\Gamma\}, \tag{3.11c}$$

$$z_2^{(-)} = \tfrac{1}{2}\{\hat{\zeta}_0 - \zeta_+ - \lambda(\zeta_0 - \zeta_-)/\Gamma\}. \tag{3.11d}$$

Thus,

$$z_1^{(+)} - z_2^{(+)} = \zeta_+ + \alpha_- \zeta_0 + \alpha_+ \zeta_-, \tag{3.12a}$$

$$z_1^{(-)} - z_2^{(-)} = \zeta_+ - \alpha_- \zeta_0 - \alpha_+ \zeta_-, \tag{3.12b}$$

$$z_1^{(+)} - z_2^{(-)} = \zeta_+ + \alpha_+ \zeta_0 + \alpha_- \zeta_-, \tag{3.12c}$$

$$z_1^{(-)} - z_2^{(+)} = \zeta_+ - \alpha_+ \zeta_0 - \alpha_- \zeta_-, \tag{3.12d}$$

where

$$\alpha_\pm \equiv (\lambda^{-1} \pm \lambda)/2\Gamma, \tag{3.13}$$

and

$$z_1^{(+)} - z_1^{(-)} = (\zeta_0 + \zeta_-)/\lambda\Gamma, \quad z_2^{(+)} - z_2^{(-)} = \lambda(\zeta_0 - \zeta_-)/\Gamma. \tag{3.12e,f}$$

The hamiltonian for two pairs then is‡

$$H_2 = (\Gamma^2/2\pi)\{\lambda^2 \ln|\zeta_0 + \zeta_-| + \lambda^{-2} \ln|\zeta_0 - \zeta_-| + \ln|(\zeta_+^2 - (\alpha_+ \zeta_0 + \alpha_- \zeta_-)^2)/(\zeta_+^2 - (\alpha_- \zeta_0 + \alpha_+ \zeta_-)^2)|\}. \tag{3.14}$$

It is clear from this expression that the dynamics of two vortex pairs is simplified when $\lambda = 1$ and/or $\zeta_0 = 0$. Indeed, for $\zeta_0 = 0$ (and any λ) the system is integrable. This may be seen in two ways. From (3.14) we have that the hamiltonian depends only on ζ_+ and ζ_-, i.e. according to (3.10) on the conjugate pairs $(Q_1^{(+)}, P_1^{(+)})$, $(Q_1^{(-)}, P_1^{(-)})$. From (2.12) we see that the additional integral

$$I = \sum_{\alpha=1}^{4} \kappa_\alpha |z_\alpha|^2 = 2\,\mathrm{Re}\,(\hat{\zeta}_0 \zeta_0^* + \zeta_+ \zeta_-^*) \tag{3.15}$$

† The variables ζ_+, ζ_- are closely related to the variables Φ, Ψ used by Domm (1956) in his analysis of the stability of vortex streets.

‡ Here and henceforth constant terms in the hamiltonian, i.e. terms independent of the vortex positions, are omitted without specific comment.

depends only on ζ_+, ζ_- for $\zeta_0 = 0$. Thus, the two-pair problem in this case reduces to a hamiltonian system with two degrees of freedom and one additional integral.

In fact this result is a special case of a more general one, namely that any four-vortex problem with vanishing total circulation and vanishing momentum is integrable. This follows from the general commutation relations of part 1 (§2):

$$[Q,P] = \sum_{\alpha=1}^{N} \kappa_\alpha, \quad [Q,I] = 2P, \quad [P,I] = -2Q \tag{3.16a–c}$$

(see (2.5), (2.6) for the definitions of Q, P and I). Thus, if the sum of the circulations vanishes, and if $Q = P = 0$, the three independent integrals Q, P and I are in involution and the four-vortex problem is integrable. This argument is more general than the one based on (3.14) and (3.15) because it applies also to cases where the vortex strengths are not opposite pairwise. A detailed analysis is given by Eckhardt (1988*b*).

When $\zeta_0 = 0$ we see from (3.10) that

$$\zeta_- = \lambda\Gamma(z_1^{(+)} - z_1^{(-)}). \tag{3.17}$$

This is the impulse carried by the pair 1^+1^-. To write equations of motion for ζ_+, ζ_- it is useful to consider the analytic continuation $\mathscr{H}_2$ of H_2, for $\zeta_0 = 0$ given by

$$\mathscr{H}_2 = (\Gamma^2/2\pi)\,[(\lambda^2+\lambda^{-2})\ln\zeta_- + \ln\{(\zeta_+^2 - (\alpha_-\zeta_-)^2)/(\zeta_+^2 - (\alpha_+\zeta_-)^2)\}]. \tag{3.18}$$

Using the Cauchy–Riemann equations we see that

$$\dot{\zeta}_+^* = (\dot{Q}_1^{(+)} - \mathrm{i}\dot{P}_1^{(-)})\sqrt{2} = (\partial H_2/\partial P_1^{(+)} + \mathrm{i}\partial H_2/\partial Q_1^{(-)})\sqrt{2} = \mathrm{i}\partial\mathscr{H}_2/\partial\zeta_- \tag{3.19a}$$

and similarly

$$\dot{\zeta}_-^* = \mathrm{i}\partial\mathscr{H}_2/\partial\zeta_+. \tag{3.19b}$$

Evaluating the derivatives in question we find

$$\dot{\zeta}_+^* = \mathrm{i}\frac{\Gamma^2}{\pi}\zeta_-\left\{\tfrac{1}{2}(\lambda^2+\lambda^{-2})\frac{1}{\zeta_-^2} + \frac{\alpha_+^2}{\zeta_+^2-(\alpha_+\zeta_-)^2} - \frac{\alpha_-^2}{\zeta_+^2-(\alpha_-\zeta_-)^2}\right\} \tag{3.20a}$$

and

$$\dot{\zeta}_-^* = -\mathrm{i}\frac{\Gamma^2}{\pi}\zeta_+\left\{\frac{1}{\zeta_+^2-(\alpha_+\zeta_-)^2} - \frac{1}{\zeta_+^2-(\alpha_-\zeta_-)^2}\right\}. \tag{3.20b}$$

The quantitative discussion of this integrable system is given in Appendix A. Some qualitative points may be found in the next subsection.

(*c*) *Some qualitative features of two-pair motion*

To uncover some of the special features of the motion of two vortex pairs it is useful to investigate various integrable limits of the dynamics. In subsection (*b*) we have already seen that there is a wide class of integrable cases. In this subsection we attempt to collect a largely qualitative synopsis of the distinguishing features that have emerged from investigations of integrable cases. Some of these features are central to an understanding of how chaos appears in this system, and what the implications of chaotic motion are.

We start with the remark that in a system where all four vortices have the same absolute value of the circulation, in our notation $\kappa_1 = \kappa_2$, a case that we shall refer to as 'identical pairs' for brevity, integrability is related to the existence of discrete symmetries, i.e. transformations forming a discrete (as opposed to continuous) group that carry the vortex configuration into

itself. For example, the integrable cases for $\zeta_0 = 0$, identified in (b) above, are associated with the existence of a centre of symmetry

$$z_1^{(s)} = -z_2^{(s)}, \quad s = \pm \tag{3.21}$$

as observed by Aref (1982). This is not true when $\kappa_1 \neq \kappa_2$. Although $\zeta_0 = 0$ now implies $z_1^{(s)} = -(\kappa_2/\kappa_1)\, z_2^{(s)}$ this is not a discrete symmetry of the equations of motion, i.e. it is not (in general) conserved under time evolution. (It *is* conserved for the steadily rotating states found in Appendix A, see (A 15).)

Another symmetry is the reflection symmetry for pairs with a common axis given by

$$z_l^{(s)} = z_l^{(-s)*}, \quad l = 1, 2; s = \pm. \tag{3.22}$$

This case has been studied extensively in the literature (Gröbli 1877, pp. 63–82; Love 1894; Hicks 1922; Friedrichs 1966, chap. 19; Acton 1976) in particular for identical pairs, with the earliest but subsequently overlooked study by Gröbli possibly being the most complete. The discrete symmetry (3.22) does extend to the case of different pairs $\kappa_1 \neq \kappa_2$ because, according to the method of images, we are solving the problem of two vortices in the vicinity of an infinite plane wall. Both symmetries (3.21) and (3.22) have extensions to more than four vortices (see Gröbli 1877; Greenhill 1878; Aref 1982).

As part of this study we have reviewed the literature on coaxial pairs and found it to be rather incomplete for $\kappa_1 \neq \kappa_2$ with a serious flaw in the most recent attempt at analysis (Acton 1976). In our analysis we have found apparently new régimes of bound-state motion for coaxial pairs of different strengths. These results and a restatement of known results for the case $\kappa_1 = \kappa_2$ are in Appendix B.

We shall see later that the greater symmetry of the case of identical pairs appears to have important consequences for the overall regularity of this system relative to the more general case of two pairs of different strengths.

States of the four-vortex system under consideration in which two or three vortices are clustered together very far from the remainder are well described, because each of the constituents is then an integrable system with a relatively simple motion (when perturbations from the distant vortex or vortices are ignored). For example, we may have a state in which the four vortices are grouped into two, distant, individually neutral, vortex pairs that never enter on a collision course. Two-vortex motion is described in any of several standard texts (see references given in §2). For a description of three-vortex motion see Gröbli (1877), Synge (1949), Novikov (1975), Aref (1979, 1983) and part 1.

We shall refer to configurations wherein all the point vortices for all time have relative displacements that remain within certain bounds as bound states. Apart from these there are three other possibilities where the vortices are paired up into freely propagating, neutral pairs either initially, finally or both. If both the initial and the final state involve such freely propagating pairs, we speak of (vortex pair) scattering, and as in other such problems use the terminology of incoming and outgoing (scattering) states. If the initial state consists of freely propagating pairs, but the final state is a bound state, we shall call the process a trapping. The converse process, which by the time reversibility of the equations of motion must also be possible, where a state remains bound for some time but then disintegrates into two vortex pairs that fly off to infinity, we shall refer to as (pair) dissolution.

Within the integrable cases it is possible to find simple examples of all these four kinds of

dynamical behaviour. For example, a head-on collision between two identical vortex pairs with a common axis of symmetry will result in a scattering process. Placing the two positive vortices close together, and, thus, by reflection symmetry the two negative vortices close together, but with sufficient separation of positive and negative vortices, will result in a bound state in which the four-vortex system simulates a vortex pair with each lobe of the pair being made up of two rapidly orbiting point vortices. Examples of trapping and dissolution can be found in the earlier paper by Aref (1982; see also Koiller *et al.* 1985). Such motions typically correspond to a separatrix in the system phase space.

Within the scattering processes a further classification is possible into what we shall call direct and exchange scattering processes, a distinction already available from the phenomenology of scattering of a pair off a single vortex in the three-vortex problem (see Aref 1979, 1983). As the names imply, a direct scattering process is one in which the incoming and outgoing pairs are the same. Using an obvious notation we might write: $(14)+(23)\rightarrow(14)^*+(23)^*$, where the * on the final states indicates that they will in general be dynamically different from the initial states. For an exchange interaction, on the other hand, we would have a 'reaction scheme': $(14)+(23)\rightarrow(13)+(24)$, which shows that the vortices have exchanged partners during the strong interaction of the collision process. The head-on collision of identical, coaxial pairs mentioned above is a simple example of this important mechanism.

Exchange scattering is strictly speaking only possible when the vortex pairs are identical. However, we shall want to use the term also in cases where $\kappa_1 \neq \kappa_2$ and an exchange of partners takes place for some long but finite time. In particular, exchange processes can lead to important nonlinear 'resonance' phenomena in cases where κ_1 and κ_2 differ by a small amount (relative to either). This observation, and the suggestion that it is important for chaotic behaviour in a four-vortex system, seems first to have been made clearly by Manakov & Shchur (1983). Similarly we shall speak of direct scattering also in those cases where two non-neutral pairs collide and re-emerge even though we know that further collisions must occur.

When two vortex pairs of nearly equal strengths collide and an exchange interaction takes place the resulting pairs will have a net circulation and thus cannot propagate to infinity. As they separate their motion can be computed from the well known formulae for a single pair. If the difference $\kappa_1-\kappa_2$ is called $\delta\kappa$, the two non-neutral pairs will move on circles of radius $\rho\sim\kappa d/\delta\kappa$ and with orbital periods $\tau\sim d^2/\delta\kappa$, where d is the separation of the vortices in the pair, which we take to be of the same order as the size of the initial pairs. In particular, as Manakov & Shchur (1983) point out, ρ is typically much larger than d because $\delta\kappa \ll \kappa_1, \kappa_2$. Also the orbital period τ can be long. These effects are easily seen in numerical experiments on vortex collisions as discussed at greater length in the following section.

4. Numerical experiments

The accessible phase space of the type of vortex system under study here is unbounded for all values of the two vortex strengths κ_1 and κ_2. Thus, except for special cases (those referred to as bound states in §3*c*) the technique of constructing Poincaré sections, a standard tool for studying non-integrable systems with bounded phase space, is not immediately available.†

† Jung (1986) has suggested an extension of the Poincaré section idea to systems with unbounded phase space, in particular those displaying 'scattering' with clearly defined 'ingoing' and 'outgoing' states. The application of this technique to the present problem is reported by Eckhardt (1988*a*).

PHILOSOPHICAL TRANSACTIONS OF THE ROYAL SOCIETY A MATHEMATICAL, PHYSICAL & ENGINEERING SCIENCES

However, the phenomenology of this problem suggests the study of scattering data such as an appropriately defined scattering angle or the 'scattering time'. Roughly speaking, the latter is the time elapsed from the initiation of 'strong interaction' between incoming pairs to the re-emergence of pairs freely propagating off to infinity, although in a system with long-range interactions this quantity is only defined in some asymptotic sense. The signal defined by the dependence of such data on initial conditions may be markedly different in different regions of phase space and for different values of the parameters κ_1 and κ_2.

In some régimes the scattering data are regular. In other régimes we have very complex data suggesting a different type of vortex motion that we call chaotic scattering. (As discussed in §5 this kind of motion is observed also in other scattering problems.) For two vortex pairs one can find régimes where the scattering process, as monitored by the dependence of scattering angle or scattering time on impact parameter, displays highly erratic behaviour. This observation was first made in a numerical experiment by Manakov & Shchur (1983). Our study provides a more comprehensive view of this interesting phenomenon including some indication of how it depends both on the ratio $\kappa_1/\kappa_2 = \lambda^2$ (see (3.9)) and on the values of the integrals of motion. By successive changes in the resolution with which we determine the initial state we provide highly suggestive numerical evidence that the scattering of two vortex pairs is truly non-integrable. Indeed we see several analogies to the observed behaviour of this system and the behaviour found in the rigorous analysis by Sitnikov of the restricted three-body problem (see Moser 1973). We argue that the case $\lambda = 1$, although still non-integrable, has regular scattering data.

We start from the obvious but, nevertheless, important remark that the asymptotics of this system are well described in terms of freely propagating pairs. When $|\zeta_+| \gg |\zeta_-|$ the hamiltonian H_2 (3.14) reduces to

$$H_2 \approx (\Gamma^2/2\pi)\{\lambda^2 \ln|\zeta_0+\zeta_-| + \lambda^{-2}\ln|\zeta_0-\zeta_-|\}. \tag{4.1}$$

According to (3.12) this hamiltonian describes two non-interacting pairs, and according to §3*a* each of these moves along a straight line. These lines can be used to define asymptotic states.

For our purposes it is sufficient to consider ingoing states with pairs moving along parallel lines. Formally (see (3.12)) this corresponds to the 'vectors' $\zeta_0+\zeta_-$ and $\zeta_0-\zeta_-$ being parallel, i.e. to

$$\mathrm{Im}\,(\zeta_0\zeta_-^*) = 0. \tag{4.2}$$

In general this quantity is not conserved during the interaction of the two pairs. However, for the integrable case $\zeta_0 = 0$ it is conserved, trivially, and so in this integrable case, identified in §3*b* and discussed further in Appendix A, we have that the outgoing pairs also propagate along parallel lines. This is also true in the case $\lambda = 1$ where exchange scattering may take place. If the outgoing pairs are the result of an exchange and we need to use (3.12*c*, *d*), then we see that the directions are again parallel because $\alpha_- = 0$ in this case, and we are assuming $\zeta_0 = 0$.

The advantage of using incoming pairs moving along parallel lines is that we can define an impact parameter geometrically as the distance between the two lines of propagation. Figure 1 shows the type of initial condition that we have used for our numerical experiments on scattering. The pairs 1^+1^- and 2^+2^- initially have separations d_1 and d_2, respectively. The separation of their midpoints is assumed much larger than both d_1 and d_2. Both pairs are tilted relative to the x-axis by an angle γ. Let

$$D \equiv \sqrt{(d_1 d_2)}; \quad \delta \equiv \sqrt{(d_1/d_2)} \tag{4.3a}$$

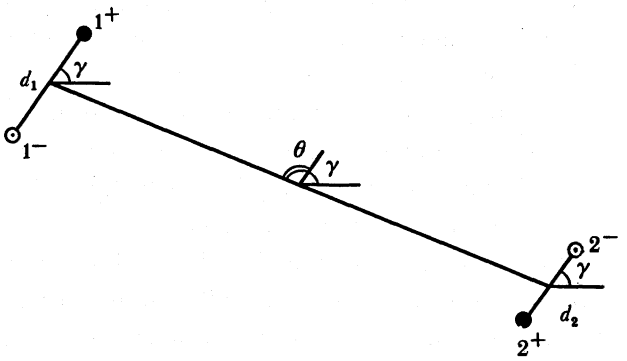

FIGURE 1. Initial condition (4.3) used in scattering experiments with vortex pairs. The distance between pair centres is assumed much greater than both d_1 and d_2.

(compare (3.9)) such that

$$d_1 = D\delta; \quad d_2 = D/\delta. \tag{4.3b}$$

The initial positions of the vortices are then given by

$$z_1^{(\pm)} = D(R\,\mathrm{e}^{\mathrm{i}\theta} \pm \tfrac{1}{2}\delta)\,\mathrm{e}^{\mathrm{i}\gamma}, \quad z_2^{(\pm)} = -D(R\,\mathrm{e}^{\mathrm{i}\theta} \pm \tfrac{1}{2}\delta^{-1})\,\mathrm{e}^{\mathrm{i}\gamma}. \tag{4.3c,d}$$

From these expressions we find

$$Q = \Gamma D\{\lambda\delta - (\lambda\delta)^{-1}\}\cos\gamma, \tag{4.4a}$$

$$P = \Gamma D\{\lambda\delta - (\lambda\delta)^{-1}\}\sin\gamma \tag{4.4b}$$

and

$$I = 2\Gamma D^2\{\lambda\delta + (\lambda\delta)^{-1}\}R\cos\theta. \tag{4.4c}$$

Thus, the integrable case $Q = P = 0$ corresponds to $\lambda\delta = 1$, or by (3.9a) and (4.3a) to

$$\kappa_1 d_1 = \kappa_2 d_2. \tag{4.5}$$

From the geometry of figure 1 the impact parameter b is given by

$$b \equiv 2DR\cos\theta. \tag{4.6}$$

For the integrable, vanishing momentum case $\lambda\delta = 1$ and

$$b = I/2\Gamma D. \tag{4.7}$$

If for fixed Γ, D, λ, δ, R and γ, we change θ, the values of the asymptotic hamiltonian H_2, (4.1), Q and P are not changed. However, such a change does alter I and thus b. In this way we can explore the entire range of impact parameters. For plotting purposes we have used a non-dimensional counterpart of I,

$$\hat{I} \equiv I/\Gamma D^2 = \{\lambda\delta + (\lambda\delta)^{-1}\}\hat{b}, \tag{4.8a}$$

where $\hat{b}$ is a dimensionless impact parameter

$$\hat{b} = b/D = 2R\cos\theta. \tag{4.8b}$$

The quantity $\hat{I}$ will be found along the abscissa in figures 2, 3, 5, 6, 7, 13, 15 and 16, and along the ordinate in figure 12.

(*a*) *Regular scattering*

We first discuss the two-pair scattering process for the integrable cases where numerical experiments can be verified by quantitative, analytical developments as given in Appendixes A and B. As discussed in Appendix A the case $Q = P = 0$ is particularly simple for $\lambda = 1$. The scattering angle, here defined as the angle through which the direction of motion of vortex 1^+ is turned by the scattering process, has been computed both by analytical theory and by direct numerical experiment. The continuous curve in figure 2 gives the analytical result as

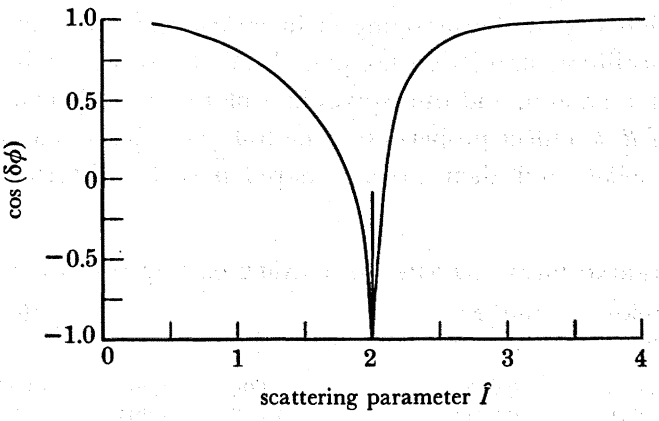

FIGURE 2. The cosine of the change in angle $\delta\phi$ (related to the scattering angle, see text) against non-dimensional parameter $\hat{I}$ for $\lambda = 1$ and $Q = P = 0$ (integrable case) from analytical results in Appendix A (see also table 1).

obtained by numerical evaluation of the formulae derived in Appendix A. The abscissa is the parameter $\hat{I}$ defined above, (4.8*a*), the ordinate is the cosine of the change in an angle ϕ introduced in Appendix A and simply related to the scattering angle (see below). We have also computed (the cosine of) this change in angle by numerical experiments in which vortex pairs were allowed to collide from an initial state of the type given in (4.3) obeying (4.5).

There is a simple connection between the scattering angle (as defined above) and the angle ϕ introduced in Appendix A or by

$$e^{i2\phi} = \zeta_-/\zeta_-^*. \tag{4.9}$$

According to (3.12*e*) the direction of motion of the pair 1^+1^- is given by $-i\zeta_-$. Hence, in a direct scattering process the net change in direction of motion for this pair equals the change in angle ϕ (see (A 3) and figure A 1). In an exchange scattering process, on the other hand, the outgoing pair will be 1^+2^- and according to (3.12*c*) its direction of motion is given by $-i\zeta_+$. From figure A 1 and (A 3) it then follows that the scattering angle will be given by the change in ϕ plus $\frac{1}{2}\pi$ (for positive p_ρ). Formulae for $\delta\phi$, the change in ϕ, are derived in Appendix A. For regular scattering when $\lambda \neq 1$ we always have direct scattering, i.e. any exchanges of partners cannot last forever, except in cases of trapping, and, thus, the scattering angle equals the change in ϕ.

The agreement between analytical and direct simulation results is traced in table 1. As explained in Appendix A the quantity that emerges naturally in the analytical expressions is $\chi = (2\Gamma/\hat{I})^2$. Hence table 1 lists cos ($\delta\phi$) as a function of χ (assuming units are chosen such that $\Gamma = 1$). The digits of all values shown in the column headed cos ($\delta\phi_{\text{analytical}}$) are all significant. To produce them we have integrated the expressions given in Appendix A using the methods

PHILOSOPHICAL TRANSACTIONS OF THE ROYAL SOCIETY A MATHEMATICAL, PHYSICAL & ENGINEERING SCIENCES

recommended by Press *et al.* (1986, chap. 4) for treating improper integrals. In the next column headed $\cos(\delta\phi_{\text{num. exp.}})$ we list values obtained by numerical scattering experiments. The degree to which we approximate the asymptotic, analytical expression for a given value of $\hat{I}$ must clearly depend on the value of R, (4.3), used in the numerical scattering experiment. Unfortunately, this dependence becomes more sensitive close to the crossover value $\chi = 1$. The values shown in table 1 were obtained with $R = 150$, a considerable initial separation for pairs of linear dimension of approximately unity. Nevertheless, considerable deviations are apparent as we approach $\chi = 1$. This is an important point for a proper appreciation of the results on 'chaotic scattering' in subsection (*b*), where we must rely entirely on numerical scattering experiments. Our position is that the mapping of incoming states (i.e. infinitely separated vortex pairs) onto 'pre-collision states' (vortex pairs headed towards each other as in (4.3) with a finite value of R) is smooth, and thus spikes in a plot of $\cos(\delta\phi)$ computed with some large but finite value of R *do* reflect properties of the full scattering dynamics, although the exact positions of the spikes and their precise shapes may be distorted in the manner exemplified by table 1.

TABLE 1. SCATTERING DATA FOR THE INTEGRABLE CASE $Q = P = 0$ AND $\lambda = 1$

χ	$\hat{I}$	$\cos(\delta\phi)$ analytical	$\cos(\delta\phi)$ numerical experiment	χ	$\hat{I}$	$\cos(\delta\phi)$ analytical	$\cos(\delta\phi)$ numerical experiment
0.2	4.472	0.998	0.998	1.005	1.995	−0.973	−0.973
0.3	3.652	0.991	0.991	1.006	1.994	−0.956	−0.956
0.4	3.162	0.975	0.975	1.007	1.993	−0.939	−0.938
0.5	2.828	0.945	0.945	1.008	1.992	−0.921	−0.920
0.6	2.582	0.889	0.889	1.009	1.991	−0.904	−0.903
0.7	2.391	0.787	0.787	1.01	1.990	−0.887	−0.886
0.8	2.236	0.594	0.594	1.02	1.980	−0.747	−0.745
0.84	2.182	0.467	0.467	1.03	1.971	−0.642	−0.640
0.88	2.132	0.287	0.287	1.04	1.961	−0.559	−0.556
0.92	2.085	0.014	0.014	1.05	1.952	−0.490	−0.487
0.96	2.041	−0.449	−0.448	1.06	1.943	−0.430	−0.428
0.98	2.020	−0.812	−0.812	1.07	1.933	−0.379	−0.376
0.99	2.010	−0.991	−0.990	1.08	1.925	−0.333	−0.330
0.991	2.009	−0.998	−0.998	1.09	1.916	−0.291	−0.288
0.992	2.008	−1.000	−1.000	1.1	1.907	−0.254	−0.251
0.993	2.007	−0.994	−0.994	1.3	1.754	0.154	0.157
0.994	2.006	−0.975	−0.976	1.5	1.633	0.339	0.342
0.995	2.005	−0.939	−0.940	1.7	1.534	0.453	0.455
0.996	2.004	−0.871	−0.876	1.9	1.451	0.531	0.533
0.997	2.003	−0.758	−0.761	2.0	1.414	0.562	0.564
0.998	2.002	−0.543	−0.550	4.0	1.000	0.808	0.809
0.999	2.001	−0.085	−0.099	6.0	0.816	0.877	0.877
1.001	1.999	−0.943	−0.942	8.0	0.707	0.909	0.910
1.002	1.998	−0.996	−0.996	10.0	0.632	0.928	0.928
1.003	1.997	−0.999	−0.999	20.0	0.447	0.965	0.965
1.004	1.996	−0.988	−0.988	30.0	0.365	0.977	0.977

To improve the agreement in table 1 one may match pre-collision initial conditions to asymptotic incoming pair states by asymptotic expansion of the equations of motion for widely separated pairs. For an application of this technique to a gravitational three-body problem see Petit & Hénon (1986) and Spirig & Waldvogel (1985).

Two further comments are in order. The first is that because the outgoing pairs for this integrable case move along parallel directions, the scattering angle can also be defined as that

angle through which the common direction of motion of the two pairs has been turned due to the scattering. Later when we discuss scattering for non-vanishing momentum, the outgoing pairs will not be moving in parallel directions. Thus, the scattering angle will always have to be defined less symmetrically as the angle through which the direction of motion of the vortex 1^+ has been turned during the interaction. This was, therefore, chosen as the basic definition.

The second comment is that although we could have integrated the reduced equations of motion for ζ_+, ζ_- as developed in §3*b*, we have chosen to integrate the full equations of motion of the vortices in their original, 'primitive' form. We have found that the reduced system is quite stiff, and thus numerically more troublesome than the primitive equations. This might have been guessed from the steep gradients in the $(r, \dot{p})$ plots of Appendix A. Except for this remark the integration of a few coupled, nonlinear, ODEs clearly does not pose any serious numerical problems. The time-stepping routines used included fourth and fifth order Runge–Kutta methods and an Adams–Bashforth predictor–corrector routine with adjustable stepsize and order. Typically the integrals Q, P, I and H were conserved to within one part in 10^5.†

The most noteworthy feature in figure 2 is the sharp singularity at $\chi = 1$. The physical interpretation of this is contained in the developments of Appendix A and is in fact already familiar from the analysis of pair-line scattering for the three-vortex problem. As discussed by Gröbli (1877) and later Aref (1979) trapping can occur for certain values of the scattering parameter corresponding to such values of the integrals that a steadily rotating state is possible. The trapping state here is one of Havelock's (1931) 'double alternating rings' mentioned in Appendix A. It lies on a separatrix between a region of direct scattering and one of exchange scattering. As $\hat{I}$ approaches a value at which trapping occurs, the scattering angle increases indefinitely. The outgoing pairs are 'thrown off' after more and more revolutions. Thus, the cosine of the scattering angle, plotted along the ordinate in figure 2, oscillates violently as we approach trapping.

The qualitative physics behind trapping is rather transparent and we want to make just two remarks. We note that this singularity in the scattering angle against impact parameter occurs for a situation that we rigorously know to be integrable. Hence, such a singularity, or a finite number of them, or even a denumerable infinity of singularities with a clear smallest separation between any two can presumably occur in an integrable scattering problem and should not uncritically be interpreted as chaos. We shall return to this issue in the next subsection. Second, we note that both in the direct and in the exchange scattering régimes the plot of scattering angle against impact parameter is smooth. It is impossible to discern from a plot such as figure 2 whether direct or exchange scattering is taking place.

We conclude this subsection by showing data for the integrable case of zero momentum with $\lambda^2 = 0.9$. A plot similar to figure 2 but this time generated exclusively by numerical scattering experiments is shown in figure 3*a*. Again we see the characteristic singularity at trapping. In figure 3*b* we show a related plot. The abscissa is again the parameter $\hat{I}$, the ordinate, however, has been changed to the scattering time, i.e. the time elapsed from 'start' to 'finish' of the scattering interaction. The operational definition is the time during which the distance between vortices 1^+ and 2^+ is less than their initial (large) separation. Because asymptotically the motion

† Subsequent confirmations at higher numerical resolution are reported by Aref *et al.* (1988).

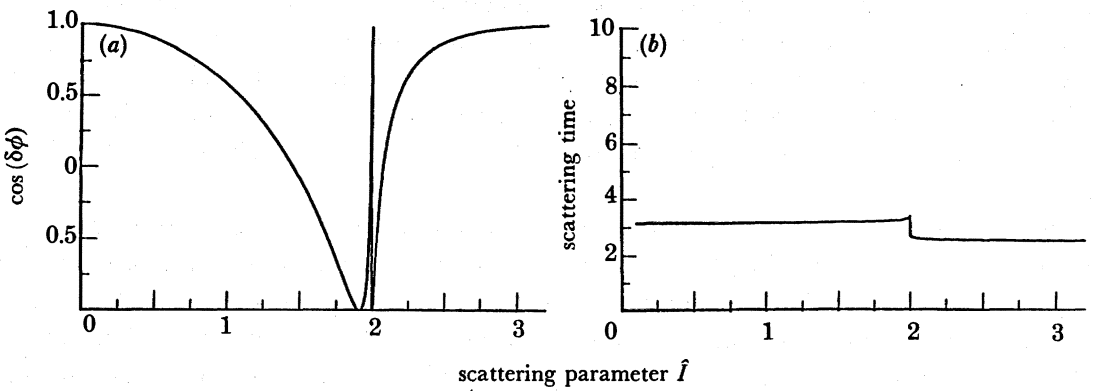

FIGURE 3. Scattering data for regular (integrable) scattering, $\lambda^2 = 0.9$, $Q = P = 0$ ($\mathscr{P} = 1$). (*a*) $\cos(\delta\phi)$ against $\hat{I}$; (*b*) scattering time against $\hat{I}$.

is linear with constant velocity, the zero point of the scale on this axis is, of course, arbitrary. By following the freely propagating pairs for longer the elapsed time can become arbitrarily large in an absolute sense. The significant aspects of figure 3*b* (and later similar figures) are the relative changes in scattering time as $\hat{I}$ is varied. Once care has been taken to be sure that initial and final states are asymptotically free, this diagnostic is extremely useful as we shall see. We see that in the exchange interaction régime (small $\hat{I}$) the scattering time is longer than in the direct scattering régime (large $\hat{I}$). There is a spike, in principle infinitely tall, at the trapping value.

To probe the physical reasons for this step-like difference in scattering times between small and large $\hat{I}$ we show in figure 4 sample trajectories of the four vortices. Panels (*a*)–(*c*) are for exchange scattering, panels (*d*)–(*f*) for direct scattering. The exchange in this case is of the 'incomplete' type described in §3*c*: the pairs try to exchange partners but cannot then escape to infinity because the intermediate pairs have non-vanishing total circulation. It is clear from figure 4 that the exchange scattering processes must take somewhat longer than the direct

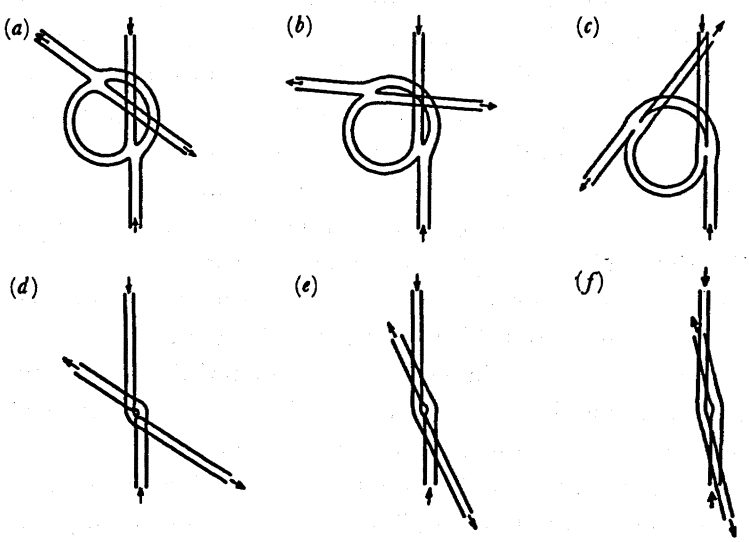

FIGURE 4. Sample trajectories of four vortices for $\lambda^2 = 0.9$ and $Q = P = 0$. Panels (*a*)–(*c*) show exchange scattering, panels (*d*)–(*f*) show direct scattering. Values of $\hat{I}$ are (*a*) 1.0; (*b*) 1.4; (*c*) 1.8; (*d*) 2.2; (*e*) 2.6; (*f*) 3.0.

scattering processes, the relative delay being due to the time it takes the intermediate pairs to complete their respective loops. Note that because we are in the integrable case the outgoing pairs always move along parallel lines.

(*b*) *Chaotic scattering*

Next we violate the condition (4.5) again for $\lambda^2 = 0.9$. We have measured the degree to which (4.5) is violated by the parameter (cf. (3.9), (4.3))

$$\mathscr{P} \equiv \lambda\delta. \tag{4.10}$$

Figure 5 shows plots of scattering angle and scattering time against impact parameter corresponding to figure 3 but for a value of $\mathscr{P} = 1.05$. Several spikes are immediately visible in both panels. As we reduce $\hat{I}$ from the direct scattering régime, the first spikes can be rationalized by appealing to the integrable case. There is again, one would assume, some kind of trapping, maybe not just into a single, steadily rotating state but into several 'channels' including various oscillations of the steadily rotating state and other periodic motions. That the situation is quite complex can be seen from figure 6 where we have gone over the scattering parameter régime at the 'upper edge' in figure 5 in more detail. The abscissa in figure 6 has been expanded by a factor 62.5 relative to figure 5. What in figure 5 seemed to be just a couple of spikes resolves itself into a complex structure of several spikes of varying heights. (Note that there is an upper cutoff on the time delay set by the duration of the computer run. The peaks reaching up to the maximum ordinate have been arbitrarily truncated at that value. Taller peaks are revealed by the increased resolution.)

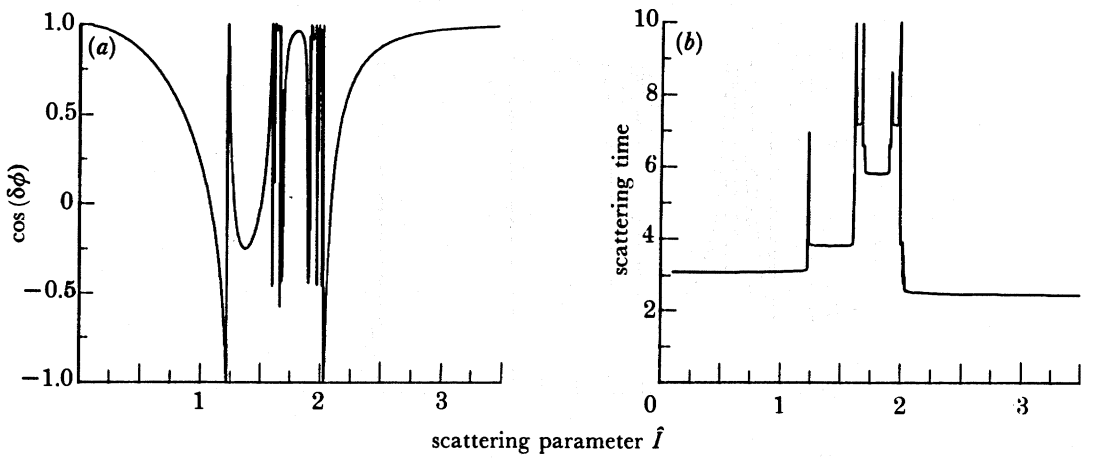

FIGURE 5. Scattering data for $\lambda^2 = 0.9$, $\mathscr{P} = 1.05$: (*a*) $\cos(\delta\phi)$ against $\hat{I}$; (*b*) scattering time against $\hat{I}$.

In figure 7 we show yet another blow-up of the scattering data. The abscissa has been expanded by an additional factor of 10 relative to figure 6, and thus in all by a factor of 625 relative to figure 5. Again considerable structure is seen in these diagnostics. One must, of course, have consistency between these various diagrams in that a feature seen in one should also appear in the expanded version(s). This test is not immediately convincing to a visual inspection. To explain this we recall the way in which this data is being generated. In each case we step with some resolution over a given interval of scattering parameter. Hence, the proximity to any particular peak will inevitably vary, and the peak may show up slightly

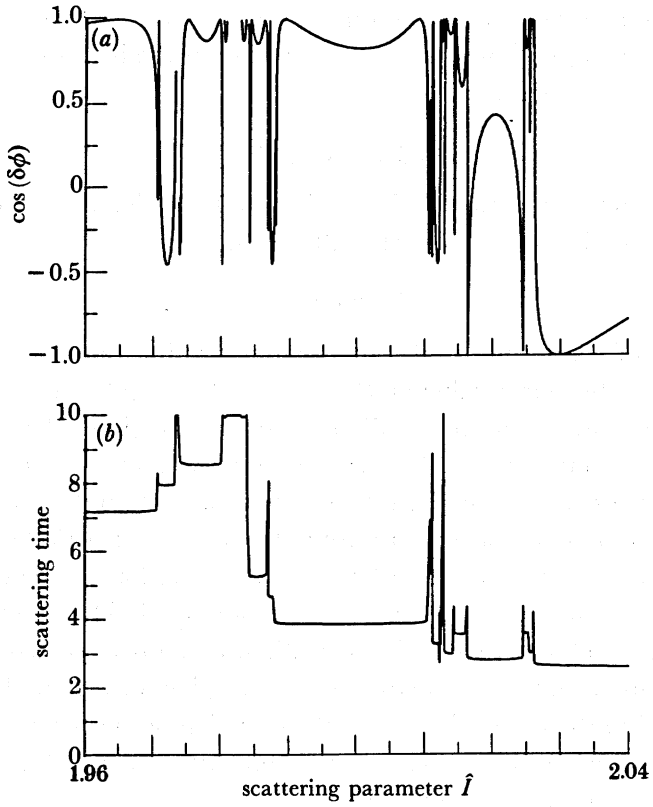

FIGURE 6. Data similar to those in figure 5 with the $\hat{I}$-axis expanded by a factor 62.5.

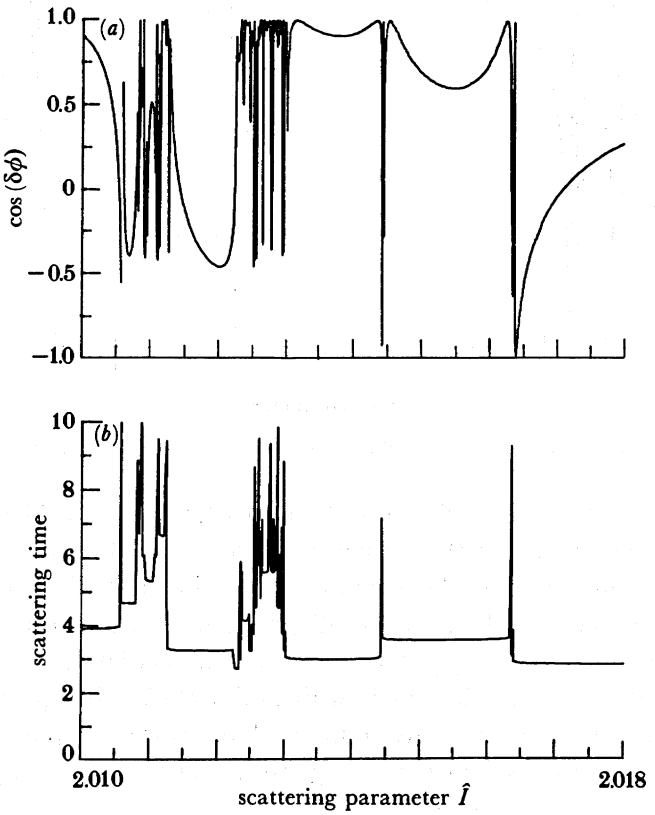

FIGURE 7. Data similar to those in figures 5 and 6 with the $\hat{I}$-axis expanded by a factor 10 relative to figure 6, 625 relative to figure 5.

PHILOSOPHICAL TRANSACTIONS OF THE ROYAL SOCIETY A MATHEMATICAL, PHYSICAL & ENGINEERING SCIENCES

displaced and with a different height on the higher resolution plot. Many additional peaks will typically emerge also. An accurate identification of individual peaks from one resolution to the next is in fact difficult even if $\hat{I}$-values are carefully duplicated when increasing the resolution (as we have also done). The overall impression of extremely complicated functions with variations on several scales of resolution in the scattering parameter $\hat{I}$ is, however, accurate and reflects the highly non-analytical character of these functions. This complexity in the scattering data is an example of chaotic scattering.

We have attempted to identify some of the physical processes responsible for the complex behaviour seen in figures 5–7. We have already seen in the integrable case the possibility of what we might call 'double exchange' interactions (figure 4, panels (*a*)–(*c*)) where the first exchange must be undone by a second before pairs can be formed that can fly off to infinity. For small $\hat{I}$ this process happens also in the non-integrable case as we expect from figure 5 and see in figure 8 (panels (*a*)–(*d*)), where trajectory plots corresponding to the scattering plot in figures 5–7 are shown.

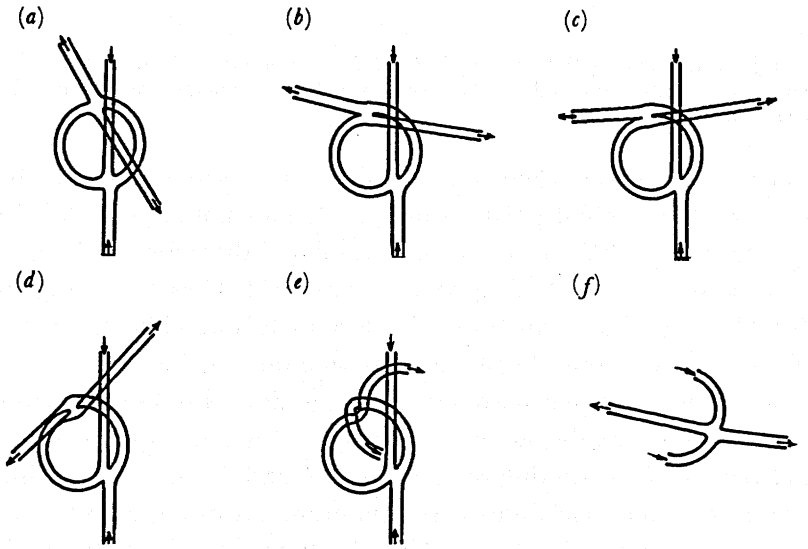

FIGURE 8. Sample trajectories of the four vortices for $\lambda^2 = 0.9$, $\mathscr{P} = 1.05$. Values of $\hat{I}$ are (*a*) 0.5; (*b*) 1.0; (*c*) 1.1; (*d*) 1.2; (*e*, *f*) 1.3. Processes in (*a*)–(*d*) are simple double exchange interactions. Process in (*e*), (*f*) is described as EDE in the text. (Panel (*f*) continues (*e*) for clarity.)

In figure 8 panels (*e*)–(*f*), however, we see a different sequence that we refer to as EDE (where E stands for 'exchange' and D for 'direct'). Panel (*e*) shows the first E and the D interaction. For clarity the second E interaction is given separately in panel (*f*). When evolutionary sequences are split between panels in this way, as we shall do on several occasions, there is usually a bit of overlap between the two panels to facilitate the conceptual continuation of the motion. The values of parameters are such that this process, possibly adorned by various oscillations, appears to be responsible for the first step in figure 5 from $\hat{I} \approx 1.25$ to $\hat{I} \approx 1.7$.

Even more exotic motions can be found in the region between the taller peaks in figure 5. Figure 9 shows one example for $\hat{I} = 1.75$. It consists of an exchange interaction followed by four direct scattering interactions and terminated by another exchange interaction undoing the first. Symbolically we write it as ED^4E.

We can speculate that an entire hierarchy of scattering 'channels' exists, where the pairs first

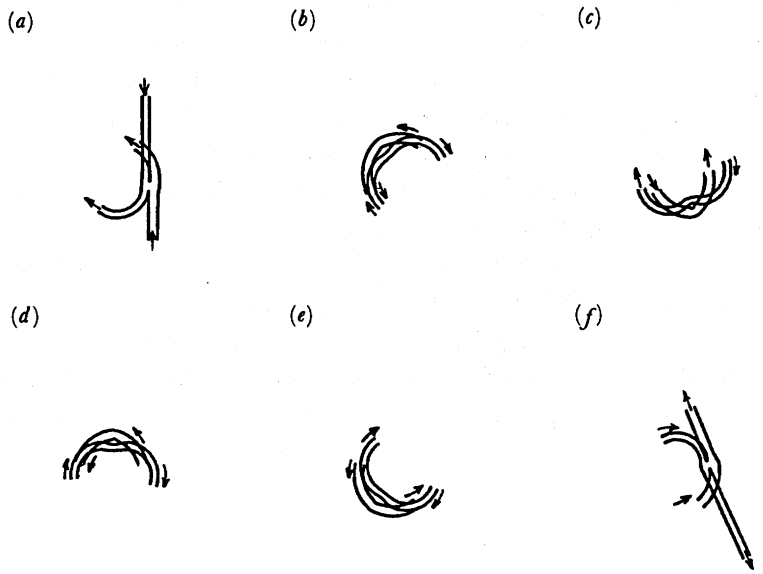

FIGURE 9. Vortex trajectories for $\lambda^2 = 0.9$, $\mathscr{P} = 1.05$, $\hat{I} = 1.75$. We observe (*a*) an exchange interaction followed (*b*)–(*e*) by four direct scatterings and (*f*) resolved by a final exchange (recombination). This process is designated ED^4E in the text.

have an exchange interaction, then several direct scatterings and finally an exchange interaction to restore the original pairs. Using an obvious notation we label these processes ED^nE, where n is an integer. We have shown examples of these for $n = 1$ (figure 8, panels (*e*) and (*f*)) and $n = 4$ (figure 9); ED^3E appears in figure 11. Clearly the suggestion that such motions exist for arbitrary n is not unreasonable. Because this step-like structure repeats on ever finer scales in $\hat{I}$, we conjecture that the plot of scattering time against impact parameter forms a so-called 'devil's staircase'. We may correlate this suggestion with the observation from figure 5 that the scattering time shows distinct steps almost as if it were 'quantized'. The difference in time delay between the E^2 scattering, seen for small $\hat{I}$, and the direct scattering of the original pairs, seen for large $\hat{I}$, is one such time delay 'quantum'. A histogram of scattering times for all the data making up a plot such as figure 6 clearly shows quantized steps with relative rarity of long values of the scattering time. Part of this suggestion is that the total time delay for given $\hat{I}$, in units of the delay 'quantum' just mentioned, is in fact just the integer n in a process ED^nE. This 'rule' seems to work for the couple of examples we have investigated in detail, but as we shall see in a moment other dynamical processes are available as well.

The picture that we have sketched here is in essence that proposed by Manakov & Shchur (1983) on the basis of more limited numerical data. We have added the important observation that the scattering data shows structure on ever finer scales in impact parameter, a feature that we feel is essential if one wants a sensible concept of chaos in a scattering problem. This feature is in some ways analogous to the issue that arises when deciding whether a numerically generated Poincaré section for a system with bounded phase space indicates chaotic behaviour or not. Any finite number of points in such a section can, in principle, lie on a contorted but smooth curve. Similarly, a finite number of numerically generated peaks in scattering time or scattering angle data could, in principle, be due to complicated but regular scattering dynamics. The appearance of new peaks at increased resolution is the more compelling evidence. The interpretation of the scattering data in terms of physical space processes,

precisely identifiable states and evolutionary patterns of the four-vortex system (as in figures 8 and 9) is an attractive feature of this problem.

As we increase $\hat{I}$ towards and slightly beyond the 'upper edge' around 2.0 in figure 5, we observe also counterparts of the trapping motions seen so clearly in the integrable case of the previous subsection. Figure 10 provides six examples of vortex trajectories as $\hat{I}$ is increased from 2.01220 to 2.01230. In panels (*a*)–(*d*) we see E^2 interactions 'topologically similar' to those in figure 8. Over a narrow range of $\hat{I}$ we then observe a transition to motions that look like finite time trapping (panels (*e*), (*f*)): the vortices all rotate rapidly about some centre only to be thrown off after a few revolutions. The evolutionary patterns (*a*)–(*d*) show a 'winding up' during the first collision as conditions come closer and closer to trapping. The type of motion seen in panels (*e*) and (*f*) of figure 10 we designate by the letter T. It seems distinct from the ED^nE sequences discussed above, although it may be a degenerate form. We note that a state of the four vortices rotating rigidly implies $Q = P = 0$. Hence these motions may only be available for small perturbations away from integrability.

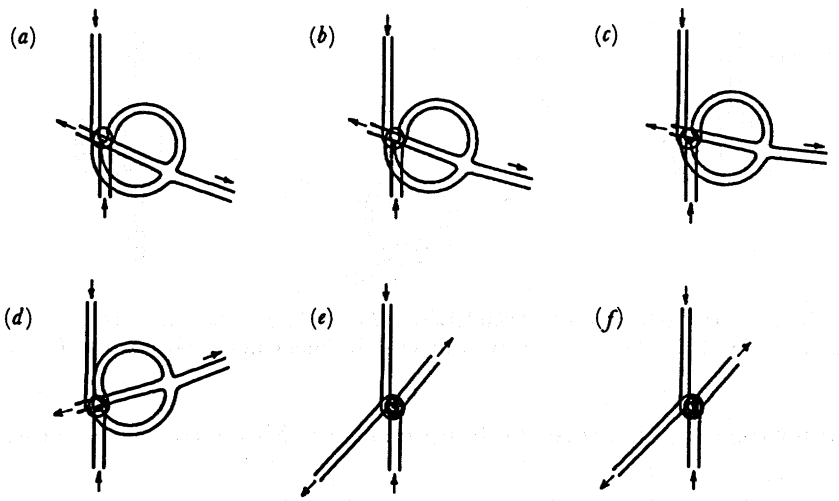

FIGURE 10. Irregular trapping occurs close to $\hat{I} = 2$. These trajectory plots are for $\lambda^2 = 0.9$, $\mathscr{P} = 1.05$. $\hat{I}$ increases in steps of 0.00002 from 2.0122 in (*a*) to 2.0123 in (*f*). Panels (*e*) and (*f*) are examples of motions designated T in the text.

Whereas the E^2 interaction for $\hat{I} = 2.0122$ yields to a T interaction as $\hat{I}$ increases, decreasing $\hat{I}$ leads to an evolutionary pattern that we would label ETE. We found that at $\hat{I} = 2.01128$ the E^2 configuration is highly symmetric (figure 11*j*). For slightly lower $\hat{I} = 2.011275$ (figure 11*h*, *i*) trapping occurs as an intermediate state leading to an ETE sequence. This in turn yields to ETDE for $\hat{I} = 2.01127$ (figure 11*e*–*g*). At lower values of $\hat{I}$ the T state becomes D^2 leading to ED^3E observed at $\hat{I} = 2.011$ (figure 11*a*–*d*). In another sequence (not shown) for $\hat{I}$ changing from 1.9880 to 1.9881 we have observed the transition EDTE → EDE. Increasing $\hat{I}$ beyond the upper limit in figure 10 we have observed the T state to spawn TD^4E for $\hat{I} = 2.01444$, TDE for $\hat{I} = 2.01445$ and TE for $\hat{I} = 2.0145$.

One may now speculate that there exist processes TD^nE and ED^nTE for arbitrary integer n, and indeed entire sequences $\ldots TD^mTD^l\ldots$, where $m, l, \ldots$ are different integers. The sequences can start and terminate with either an E or T interaction. These possibilities suggest also how one can introduce a symbolic dynamics for this scattering problem of the same general

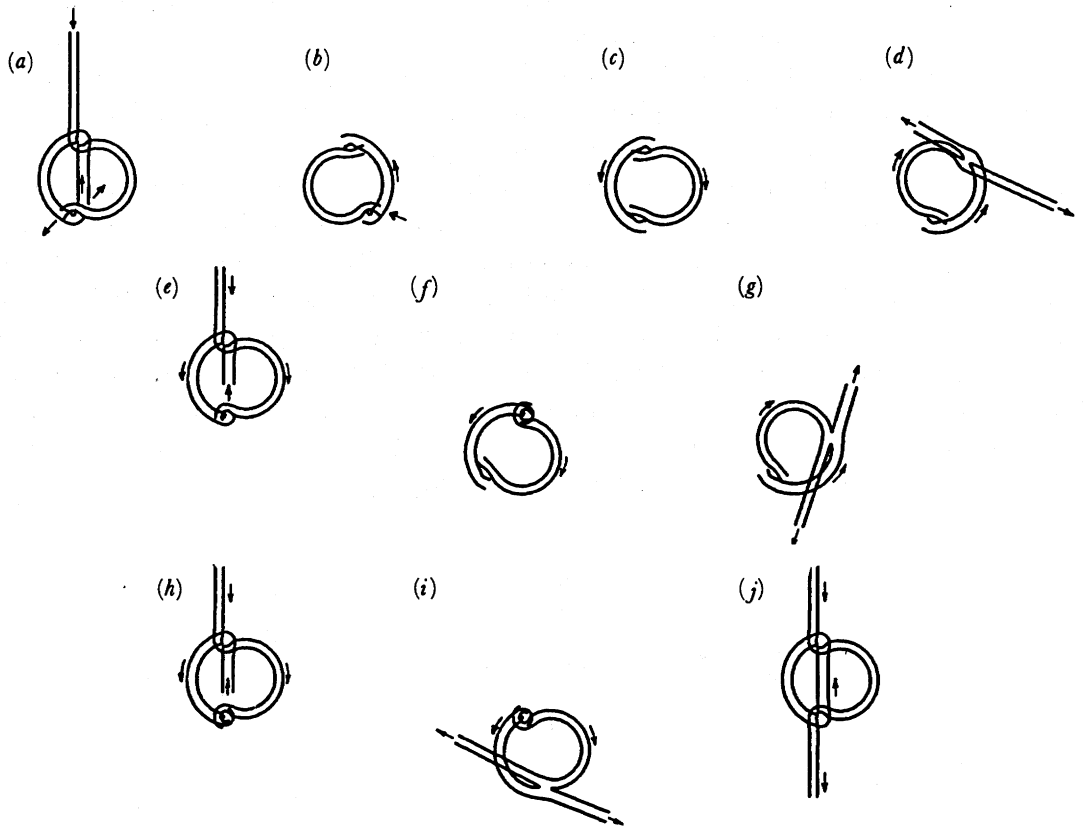

FIGURE 11. Transition for $\lambda^2 = 0.9$, $\mathscr{P} = 1.05$ from ED^{3}E at $\hat{I} = 2.011$ ((*a*)–(*d*)) to ETDE at $\hat{I} = 2.01127$ ((*e*)–(*g*)) and ETE at $\hat{I} = 2.011275$ ((*h*)–(*i*)). A very symmetric E^2 interaction is observed at $\hat{I} = 2.01128$ (*j*).

nature as that for the restricted three-body problem (see Moser 1973). For now, however, the details are sketchy.

The hierarchy of interactions explains the origin of the fractal structure seen in the scattering data. When we have an entire sequence of interactions, e.g. ETD^{3}E, the initial value of $\hat{I}$ selects whether we start off with E or T. However, once that choice has been made this first interaction stays essentially the same and the sensitivity to small changes of $\hat{I}$ is transferred to the selection of whether the second interaction should be an E, D or T. (In figure 11, for example, the initial E interaction is virtually identical in panels (*a*), (*e*), (*h*) and (*j*). The second interaction varies from D to T to E.) In this way a finite interval of $\hat{I}$ is 'mapped' onto smaller intervals of the impact parameter characterizing the second interaction process. If this second process is D or T, further sensitivity is available. The interval of impact parameters for the second interaction, and thus $\hat{I}$, is then further subdivided according to different possibilities for the third interaction, and so on.

We have explored the scattering data for $\lambda^2 = 0.9$ and various values of $\mathscr{P}$, (4.10). As shown above a 5% increase of this ratio above the integrable value $\mathscr{P} = 1$ results in highly complex scattering data that we have associated with chaotic behaviour. A corresponding decrease of 5% in $\mathscr{P}$ to 0.95, however, results in apparently smooth scattering data differing very little from figure 3. Not until we reach $\mathscr{P} \approx 0.8$ do we begin to see complex structure in scattering data comparable to figure 5. We have no immediate explanation of this asymmetry.

Figure 12 is a crude attempt to summarize several plots of the type shown in figure 5. Along the abscissa we have the ratio $\mathscr{P}$, along the ordinate the scattering parameter $\hat{I}$, with the interval where complex structure of scattering data is observed shown by a vertical bar. The width of this region vanishes at $\mathscr{P} = 1$, and as we have just mentioned widens considerably more quickly on the side $\mathscr{P} > 1$ than on the side $\mathscr{P} < 1$. Of course within each $\hat{I}$-interval there are typically gaps, where the variation of scattering data is quite smooth, separated by thin regions with peaks and violent variations. Our bar graph in figure 12 does not reflect this fine structure.

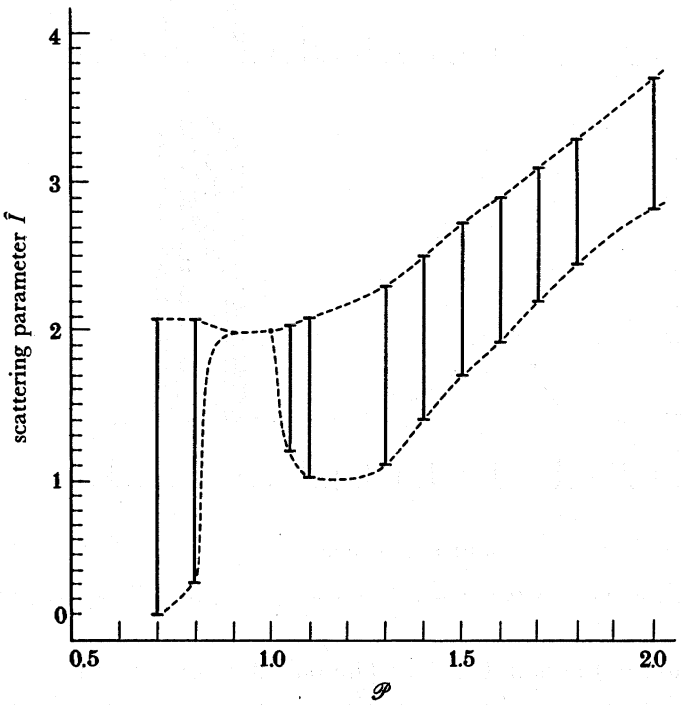

FIGURE 12. A plot of the interval in $\hat{I}$ for which irregular scattering data are observed as a function of $\mathscr{P}$ for $\lambda^2 = 0.9$.

When the ratio $\mathscr{P}$ is increased far beyond unity, plots of scattering data change character. Figure 13 shows scattering angle and time against $\hat{I}$ for $\mathscr{P} = 2.2$. The step-like appearance of the scattering time is no longer in evidence, and the window of chaotic scattering is considerably narrower. For this value of $\mathscr{P}$ we have initially one pair of closely bound, strong vortices (2^+2^-) and one pair of widely separated weaker ones (1^+1^-). It is therefore natural to interpret these data in terms of collisions of a vortex pair with a single vortex in the field of a more distant second vortex. Figure 14 shows vortex trajectories corresponding to the data in figure 13. The tightly bound pair (2^+2^-) impinges on one of the vortices (1^+) in the loose pair. A brief exchange interaction takes place and a small loop traced out by 2^-1^+ is visible. Another exchange interaction reproduces the original pairs. The wide bump for small $\hat{I}$ in figure 13*b* is due to the two outgoing pairs propagating side by side for some time before becoming asymptotically free.

For $\hat{I} \approx 3.72$, in the middle of the chaotic régime seen in figure 13, we found the following complicated motion (figure 14, panels (*d*)–(*h*)). (*d*) The pair 2^+2^- collides with 1^+. Two non-neutral pairs 2^-1^+ and 2^+1^- are formed. The latter pair has a separation approximately equal

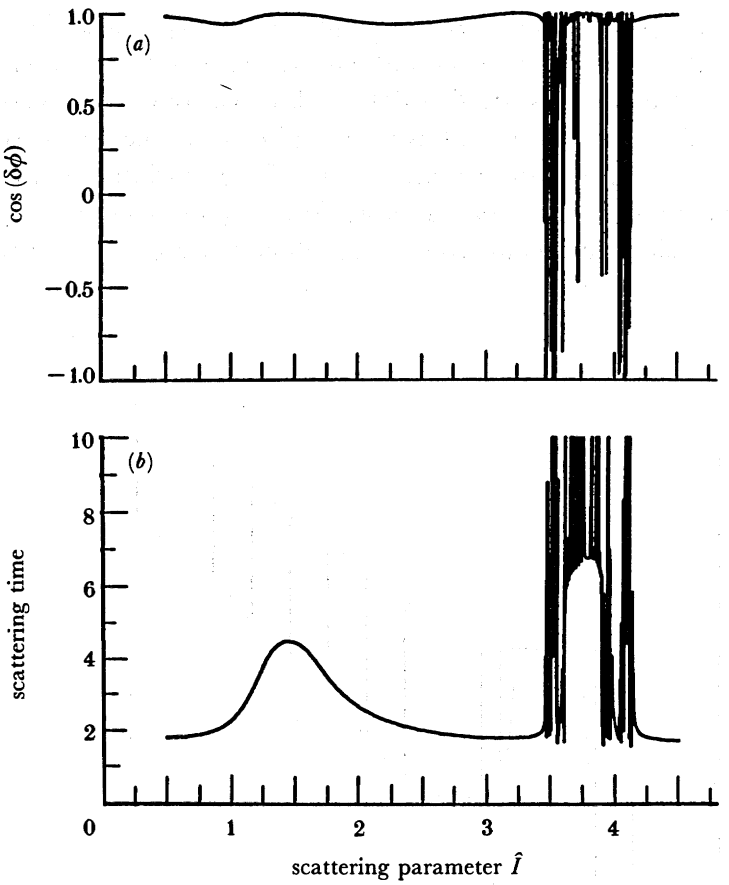

FIGURE 13. Scattering data for $\lambda^2 = 0.9$, $\mathscr{P} = 2.2$: (*a*) cos ($\delta\phi$) against $\hat{I}$; (*b*) scattering time against $\hat{I}$.

to the original separation of the pair 1^+1^-. (*e*) The pair 2^+1^- orbits on a large circle. The pair 2^-1^+ orbits a smaller circle because the size of this pair when it is formed is much smaller. The pair 2^-1^+ completes many orbits (about 30; the solid black 'apple-shaped' region), whereas the pair 2^+1^- completes one. (*f*) As all four vortices approach several direct scatterings take place. (*g*) The pair 2^+1^- re-emerges for another large circle orbit. The pair 2^-1^+ again completes several cycles (about nine) of a precessing circular orbit of smaller radius. (*h*) At the next close aproach of all vortices an exchange interaction re-ejects the original pairs.

This particular sequence exemplifies the possibilities for chaos in this parameter régime. Tiny changes in impact parameter can now trigger different ratios of orbital frequencies for the two pairs set up by the initial exchange. In turn the ratio of orbital frequencies determines the ultimate angles at which pairs re-emerge from the scattering region. In the chaotic régime the scattering angle again becomes a random function of scattering parameter.

As a final view of the variation of scattering data with system parameters we show in figure 15 plots of the scattering time against impact parameter for $\mathscr{P} = 1.1$ and $\lambda^2 = 0.95$, 0.9 and 0.8. The range of $\hat{I}$-values leading to chaotic scattering clearly decreases with λ. We also observe that the steps in the scattering time decrease with λ. One can rationalize these observations by noting that as $\lambda \to 0$ one pair becomes simply a passive advectant in the velocity field of the other. In this limit there is no chaos. The surprise is that this effect is observable at such a large value of λ^2 as 0.8.

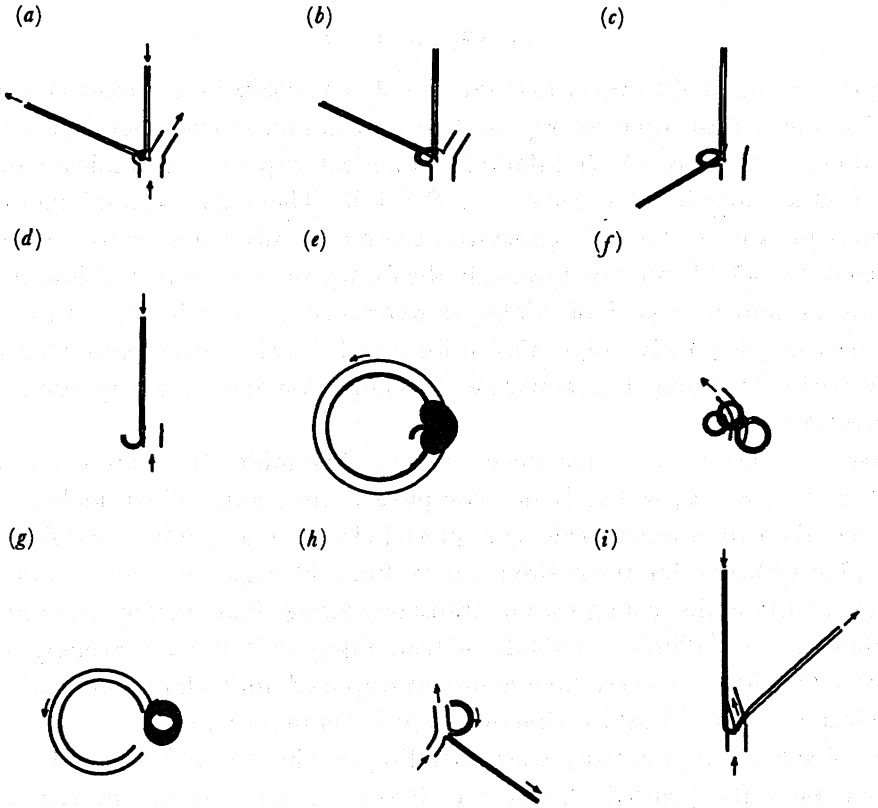

FIGURE 14. Vortex trajectories for $\lambda^2 = 0.9$, $\mathscr{P} = 2.2$ and (*a*) $\hat{I} = 1.0$; (*b*) 2.0; (*c*) 3.0; (*d*)–(*h*) 3.72; (*i*) 4.0. The complicated sequence (*d*)–(*h*) is explained in the text.

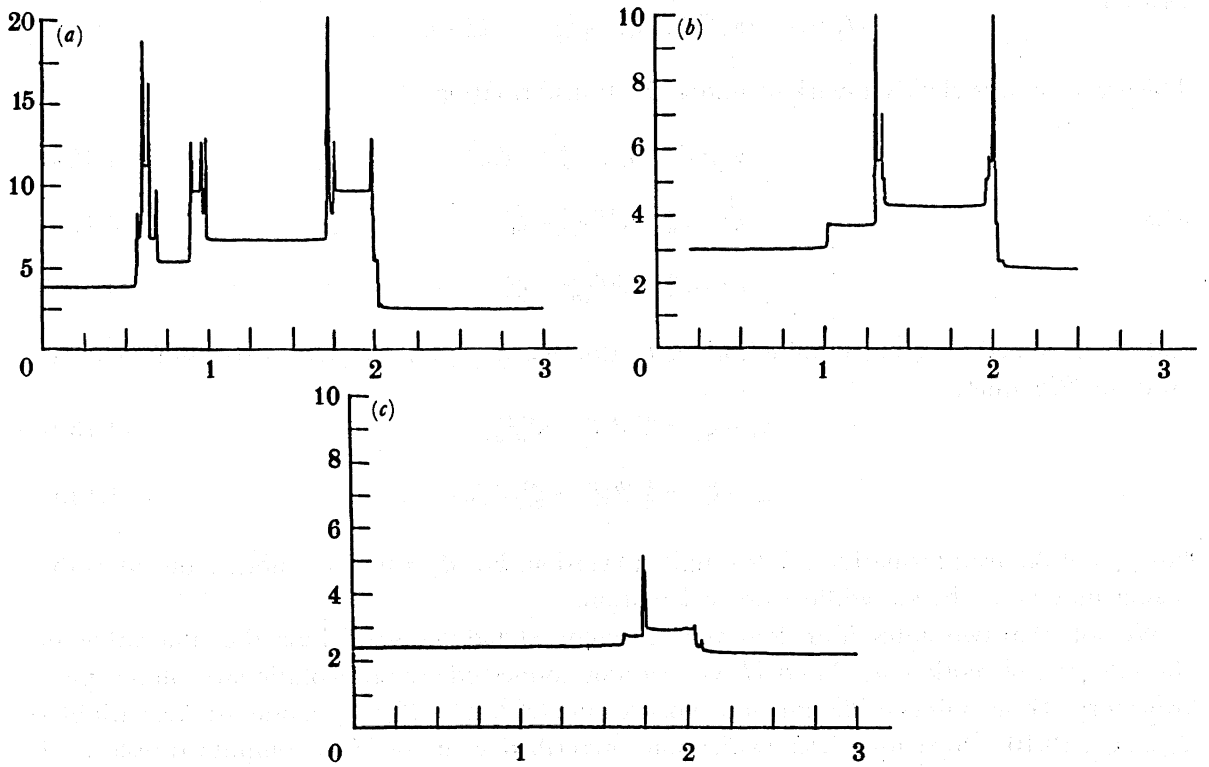

FIGURE 15. Scattering time against impact parameter for $\mathscr{P} = 1.1$ and (*a*) $\lambda^2 = 0.95$; (*b*) 0.9; (*c*) 0.8.

(c) *The case* $\lambda = 1$

From figure 15 one might expect that the case $\lambda = 1$ would be the most violently chaotic: the two pairs enter on an equal footing, and because complete exchange is possible, peaks in scattering times can easily reach infinity. Numerical experiments indicate otherwise. In figure 16 we show scattering data for $\lambda = 1$, $\mathscr{P} = 1.05$. There is no hint of chaotic scattering. From our previous investigations a qualitative reason for this is not far to seek. The essential ingredient that is available for $\lambda \neq 1$, namely the formation of non-neutral intermediate pairs, that can loop around in a kind of nonlinear resonance, as seen in several examples in the previous subsection, is simply not available for $\lambda = 1$. Evolutionary patterns such as ED^nE above cannot arise. Exchange interactions go to completion and the newly formed pairs fly off never to interact again.

Nevertheless, so far as we have been able to determine the four-vortex system with circulations $\kappa_1 = \kappa_2 = -\kappa_3 = -\kappa_4$ is not completely integrable. If we look at bound-state motions, where the two positive vortices are placed close to one another, and the two negative vortices are placed closely, but the positives are far from the negatives, the vortices of either sign stay together as the entire configuration translates along. Numerically generated Poincaré sections (with several different methods of sectioning) in this case strongly suggest non-integrability. A detailed report on these results is postponed until a later publication. However, as we have just seen, the scattering dynamics appear entirely regular.

We do not have a comprehensive understanding of why the problem with $\lambda = 1$ appears more regular than the general case $\lambda \neq 1$. However, we have discovered a continuous symmetry of the transformed hamiltonian (3.14) that apparently hinges on special groupings and cancellations that occur for $\lambda = 1$. For $\lambda = 1$ (and $\Gamma = 1$) the hamiltonian can be written

$$H_2 = -(2\pi)^{-1} \ln|(\zeta_0^2 - \zeta_-^2)^{-1} - (\zeta_0^2 - \zeta_+^2)^{-1}|. \tag{4.11}$$

This expression is clearly invariant under the transformation

$$\mathscr{T}_\Psi : \zeta_+ \to \tilde{\zeta}_+, \quad \zeta_- \to \tilde{\zeta}_-, \tag{4.12a}$$

where

$$\tilde{\zeta}_+^2 - \zeta_0^2 = e^{i\Psi}(\zeta_+^2 - \zeta_0^2), \tag{4.12b}$$

$$\tilde{\zeta}_-^2 - \zeta_0^2 = e^{i\Psi}(\zeta_-^2 - \zeta_0^2) \tag{4.12c}$$

and Ψ is assumed real. The infinitesimal generator of $\mathscr{T}_\Psi$ is given by (4.12) expanded to linear order in Ψ, namely

$$\tilde{\zeta}_+ - \zeta_+ = \tfrac{1}{2} i \Psi(\zeta_+ - \zeta_0^2/\zeta_+), \tag{4.13a}$$

$$\tilde{\zeta}_- - \zeta_- = \tfrac{1}{2} i \Psi(\zeta_- - \zeta_0^2/\zeta_-). \tag{4.13b}$$

For $\zeta_0 = 0$ the transformation $\mathscr{T}_\Psi$ is simply a rotation. For $\zeta_0 \neq 0$, $\mathscr{T}_\Psi$ is not canonical as the reader may verify by straightforward calculation.

We note that two states of the four-vortex system related via (4.12) have the same values of the integrals of motion Q, P and H, yet are not connected by an evolutionary phase space trajectory. To see this consider any four-vortex state $(z_1^{(+)}, z_1^{(-)}, z_2^{(+)}, z_2^{(-)})$. Compute the variables $\zeta_0, \hat{\zeta}_0, \zeta_\pm$, (3.10). Next use (4.12) with some prescribed value of Ψ to compute transformed

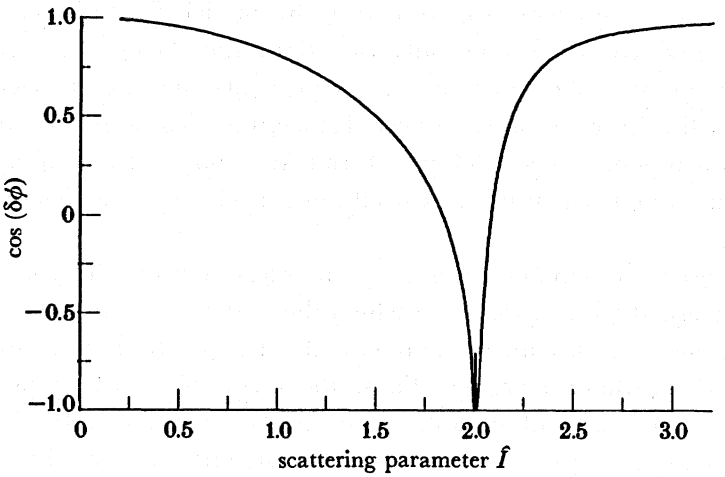

FIGURE 16. Scattering data for $\mathscr{P} = 1.05$ and $\lambda = 1$. This plot should be compared with figures 5–7.

variables $\tilde{\zeta}_\pm$ (retain ζ_0 and $\hat{\zeta}_0$). Now use the inverse formulae (3.11) (with both λ and Γ set to unity) to compute a new four-vortex state

$$(\tilde{z}_1^{(+)}, \tilde{z}_1^{(-)}, \tilde{z}_2^{(+)}, \tilde{z}_2^{(-)}) \equiv \mathscr{T}_\Psi(z_1^{(+)}, z_1^{(-)}, z_2^{(+)}, z_2^{(-)}) \tag{4.14}$$

from ζ_0, $\hat{\zeta}_0$ and the transformed $\tilde{\zeta}_\pm$. Except for special values of Ψ and/or the integrals of motion the two states $(z_1^{(+)}, z_1^{(-)}, z_2^{(+)}, z_2^{(-)})$ and $(\tilde{z}_1^{(+)}, \tilde{z}_1^{(-)}, \tilde{z}_2^{(+)}, \tilde{z}_2^{(-)})$ will be different. The integral I will, clearly, be preserved under this transformation when $\zeta_0 = 0$. When $\zeta_0 \neq 0$, I depends on the position of the origin of coordinates and we can arrange that $I = 0$ and $\tilde{I} = 0$ by a simple shift of coordinates (which does not alter the values of Q, P and H).

We envisage that the relative regularity of the $\lambda = 1$ case is due to the existence of this transformation which might establish a one-to-one correspondence between scattering states that are not related by time evolution. However, we do not see in detail how such a reduction of the problem comes about.

5. Concluding remarks

Vortex pairs are readily produced in two-dimensional flows and a variety of dipole vortices, for which the point vortex pair is the simplest model, have been studied extensively in connection with laboratory and geophysical flows. Vortex-pair formation has been studied via numerical simulations by Aref & Siggia (1981), Aref (1982), McWilliams (1984), and others, and via simulation and laboratory experiment by Couder & Basdevant (1986). Vortex-pair collisions were attempted in a laboratory experiment by Tatsuno & Honji (1977) and more recently by Couder & Basdevant (1986). For the finite-area counterpart of the integrable, coaxial pair collisions precision computations have been published by Overman & Zabusky (1982) and by McWilliams & Zabusky (1982). The closely related problem of vortex pairs in a two-layer fluid has been considered by Hogg & Stommel (1985*a*, *b*) who call such entities hetons. In the numerical experiments performed by these authors many features analogous to those seen in the simpler point vortex model are apparent. All these examples show that the dynamics of interacting vortex pairs is of considerable importance as a basic ingredient in more complicated flows.

One of the main inadequacies of the point vortex model relative to more realistic finite-core

vortices is that vortex merging events are ignored in this model. Real discrete vortices of the same sign will frequently orbit each other only for a finite time before a merging event takes place that reduces the number of distinct vortices by (at least) one. Like-signed point vortices, on the other hand, will orbit each other forever. Hence, the chaotic motion observed in the problem of four identical point vortices (cf. part 1 and Aref 1985) may be of limited relevance to applications because isolated real vortices would not survive for a sufficient length of time to observe the effect.

The form of chaos observed here, however, may suffer less from this drawback. In scattering problems we are concerned with processes in which the vortex pairs interact for a finite time with only a few close encounters. Pairs of discrete, real vortices with finite cores could possibly survive such sequences without merging. Thus, the chaos observed in point vortex-pair interactions may have more easily observable counterparts in real fluids. In view of the results of numerical and laboratory experiments on two-dimensional flows (see the references given above) where vortex pairs are observed in abundance, the mechanisms documented here are thus likely to be important for an understanding of chaotic and, maybe, ultimately turbulent behaviour. The details of how chaos observed in deterministic few-vortex models is related to statistical flow régimes in conventional shear flows is, of course, still a formidable challenge (cf. Aref *et al.* 1987).

We mention that the notion of chaotic scattering pursued here for vortices appears to be a general feature of open systems in which intermediate complexes of long but finite lifetime can be formed. In the vortex system $(\pm\kappa_1, \pm\kappa_2)$ with $\kappa_1 \neq \kappa_2$ these intermediate complexes are the pairs $(+\kappa_1, -\kappa_2), (-\kappa_1, +\kappa_2)$. This terminology is borrowed from chemical physics where phenomena closely analogous to what we observe in this classical, fluid-mechanical system have been demonstrated. For example, Noid *et al.* (1986) report apparently fractal scattering data in numerical experiments on a two degree of freedom model of $He+I_2$ collisions. Earlier work includes papers by Gottdiener (1975) and Agmon (1984). One of the earliest references is Rankin & Miller (1971). The term chattering has been introduced for such phenomena, an obvious concatenation of chaotic scattering. Chattering in the gravitational three-body problem has been discussed by Spirig & Waldvogel (1985) and by Petit & Hénon (1986). Eckhardt & Jung (1986) have observed chaos in scattering of a particle by an exponentially damped Hénon–Heiles type potential. Campbell *et al.* (1986) discuss regular and irregular behaviour for kink–antikink interactions in the Sine–Gordon equation. Recently Eckhardt (1987) has considered elastic scattering (reflection) of a ray off three cylinders arranged in an equilateral triangle. The chaotic scattering observed here suggests applications of the concept to the topic of ray tracing.

We anticipate that chaos in scattering problems is a widespread phenomenon and that many examples will be discovered and discussed in the near future. In many instances this type of chaos is at least as important for applications as the well-studied case of chaos in systems with bounded phase space. It is gratifying that the classical point vortex model of Helmholtz provides the first example of chaos in a scattering problem of relevance to fluid mechanics.

H. A. is indebted to Dr N. Pomphrey for contributions to this problem, in particular portions of the analysis of integrable cases, dating from 1980 to 1981. B. E. thanks Professor P. H. Richter and Dr C. Jung for discussions.

A first version of this paper was written while H. A. was a visiting professor at Laboratoriet

for Anvendt Matematisk Fysik (LAMF), Technical University of Denmark, supported by the Danish Council for Industrial and Scientific Research under grant 16-3862. We are both indebted to the members of LAMF for their hospitality.

This work is supported in part by DARPA/ACMP under URI grant N00014-86-K-0758 administered by ONR, and in part by NSF/PYI grant MSM84-51107. Industrial matching funds for the latter have been generously contributed by General Electric Company, Ametek Computer Research Division, Sundstrand Turbomach and Cray Research.

Appendix A. The integrable case $Q = P = 0$

The hamiltonian is $\mathrm{Re}\,\mathscr{H}_2$, (3.18), or

$$H_2(\zeta_0 = 0) = (\Gamma^2/2\pi)\{(\lambda^2+\lambda^{-2})\ln|\zeta_-| + \ln|(\zeta_+^2-(\alpha_-\zeta_-)^2)/(\zeta_+^2-(\alpha_+\zeta_-)^2)|\}. \tag{A 1}$$

From (3.17) we know that the key variable is ζ_- and from (3.15) that

$$I = 2\,\mathrm{Re}\,(\zeta_+\zeta_-^*). \tag{A 2}$$

is an integral of the motion. These observations lead us to the canonical transformation

$$\zeta_- = \rho\,\mathrm{e}^{\mathrm{i}\phi}; \quad \zeta_+ = -(p_\phi/\rho - \mathrm{i}p_\rho)\,\mathrm{e}^{\mathrm{i}\phi}. \tag{A 3}$$

The canonical commutation relations:

$$[\rho, p_\rho] = [\phi, p_\phi] = 1 \tag{A 4}$$

(all remaining Poisson brackets vanish) are equivalent to

$$[\zeta_+, \zeta_-] = 0; \quad [\zeta_+, \zeta_-^*] = -2\mathrm{i}. \tag{A 5}$$

Substitution of (A 3) into (A 1) gives

$$\rho^{2(\lambda^2+\lambda^{-2})}\{(p_\phi^2-(\rho p_\rho)^2-\alpha_-^2\rho^4)^2+4(\rho p_\rho\, p_\phi)^2\} = \mathscr{k}\{(p_\phi^2-(\rho p_\rho)^2-\alpha_+^2\rho^4)^2+4(\rho p_\rho\, p_\phi)^2\}, \tag{A 6}$$

where

$$\mathscr{k} = \exp(4\pi H_2/\Gamma^2) \tag{A 7}$$

and where, according to (A 3) and (A 2)

$$p_\phi = -\mathrm{Re}\,(\zeta_+\zeta_-^*) = -\tfrac{1}{2}I \tag{A 8}$$

is an integral. The hamiltonian (A 1) does not depend on its conjugate variable ϕ.

A 'phase plane' analysis of this system is now obtained by introducing variables

$$r = \rho^2/|p_\phi|, \quad p = p_\rho^2/|p_\phi| \tag{A 9}$$

and plotting level curves of

$$r^{\lambda^2+\lambda^{-2}}\frac{(1-rp-\alpha_-^2 r^2)^2+4rp}{(1-rp-\alpha_+^2 r^2)^2+4rp} = \chi, \tag{A 10}$$

where

$$\chi = \mathscr{k}/|\tfrac{1}{2}I|^{\lambda^2+\lambda^{-2}}. \tag{A 11}$$

This is most easily done by noting that (A 10) is a quadratic polynomial in $x \equiv rp$. To write it in a convenient form let

$$a_n = \alpha_+^{2n}\chi - \alpha_-^{2n} r^{\lambda^2+\lambda^{-2}} \tag{A 12}$$

for $n = 0, 1, 2$ and note that

$$a_2 = (\alpha_+^2 + \alpha_-^2)\, a_1 - (\alpha_+ \alpha_-)^2\, a_0. \tag{A 13}$$

Then (A 10) becomes

$$ax^2 + bx + c = 0, \tag{A 14a}$$

where

$$a = a_0, \tag{A 14b}$$

$$b = 2(a_0 + a_1 r^2), \tag{A 14c}$$

$$c = a_0 - 2a_1 r^2 + a_2 r^4, \tag{A 14d}$$

$$= a_0\{1 - (\alpha_+ \alpha_-)^2 r^4\} + a_1\{(\alpha_+^2 + \alpha_-^2) r^2 - 2\} r^2.$$

Figure A 1 shows the (r, p) phase diagram for $\lambda = 1$. (For clarity of presentation we actually plot p against $\ln r$.) In this particular case (A 10) simplifies considerably. Figure A 2 shows a corresponding diagram for $\lambda^2 = 0.9$. It is easier to discuss this 'generic' plot first and then return to figure A 1 as a limiting case. We clearly see that the plot in figure A 2 is dominated by three singular points, two elliptic fixed points on the r-axis and a hyperbolic (saddle) point away from that axis. The two elliptic points can be easily understood from (A 10). One corresponds to $\alpha_- r = 1$, the other to $\alpha_+ r = 1$. The values of χ are 0 and ∞, respectively. These points correspond to singular limits of the dynamics. The hyperbolic point, on the other hand, is entirely accessible and corresponds to a steadily rotating state of the four-vortex system. The diagram shows that this state is unstable because it is on a separatrix extending to infinity. Physically the uniformly rotating state can disintegrate into two freely propagating pairs. Some of these motions correspond to trapping in two-pair scattering as described in §§3*c* and 4*a*. For the integrable case under discussion here this trapping is analytically calculable. In practice, however, the resulting formulae are extremely complicated.

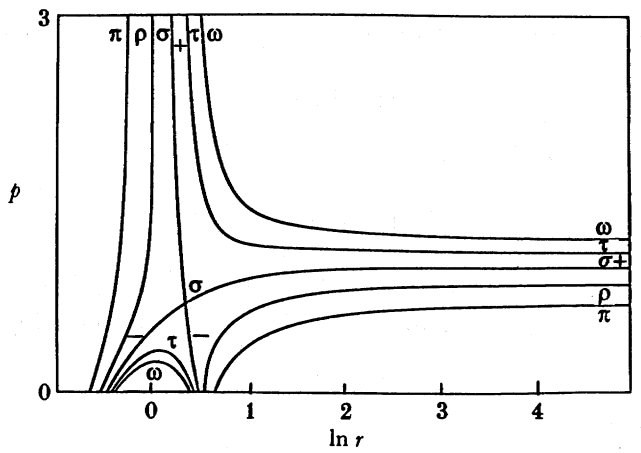

FIGURE A 1. 'Phase plane' trajectories for pairs with vanishing momentum and $\lambda = 1$. The classes of curves labelled π, ρ, σ, τ, ω and the $\pm$ signs are explained in the text.

We have found the steady states directly in a straightforward if somewhat tedious calculation that will not be reproduced here. The result is that these states are given by the parametric representation

$$z_1^{(\pm)} = s[2\lambda\, e^{i\Omega} \pm (1 + \lambda^2)\, \xi]; \quad z_2^{(\pm)} = -\lambda^2 z_1^{(\pm)}, \tag{A 15a}$$

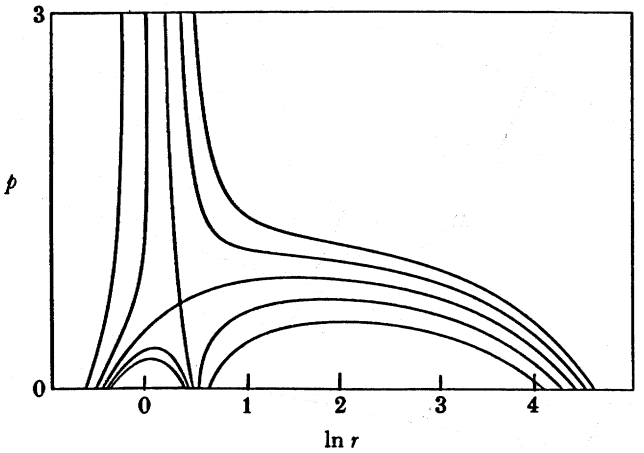

FIGURE A 2. A 'phase plane' diagram similar to that in figure A 1 but for $\lambda < 1$ (actually $\lambda^2 = 0.9$).

where s is a free parameter that sets an overall scale for the configuration and the speed of rotation,

$$\xi^2 = 2\Lambda/[1+\sqrt{(\Lambda^4-\Lambda^2+1)}] \tag{A 15b}$$

with

$$\Lambda \equiv \tfrac{1}{2}(\lambda^2+\lambda^{-2}) \tag{A 15c}$$

and

$$\cos(2\Omega) = [-1+\sqrt{(\Lambda^4-\Lambda^2+1)}]/\Lambda^2. \tag{A 15d}$$

The configuration rotates about the point of intersection of 1^+2^+ and 1^-2^- (chosen as the origin in (A 15a)). The corresponding value of χ is

$$\chi_c = \left(\frac{4\Lambda}{1+\sqrt{(\Lambda^4-\Lambda^2+1)}}\right)^{\Lambda} \frac{\Lambda+\sqrt{(\Lambda^4-\Lambda^2+1)}}{(\Lambda+1)^2}. \tag{A 15e}$$

Note that for $\lambda = 1$, we have $\Lambda = 1$, $\xi = 1$, $\Omega = \frac{1}{4}\pi$ (or $\frac{3}{4}\pi$) and $\chi_c = 1$. Also note that in figure A 2 the elliptic fixed point at $p = 0$, $r = 1/\alpha_-$ moves off to $r = \infty$. Hence, figure A 2 becomes figure A 1.

Samples of the steady states given parametrically above are plotted in figure A 3 for various values of λ. The case $\lambda = 1$ leads to the smallest of a family of states discussed already by Havelock (1931) and called by him 'double alternate rings'. In the rhombus that arises for $\lambda = 1$ the opening angle is $\frac{1}{4}\pi$.

The phase plane analysis gives an overall view of the various possible régimes of motion. To make detailed quantitative statements on time evolution we must return to the equations of motion such as

$$\dot{\phi} = \partial H_2/\partial p_\phi. \tag{A 16}$$

This equation gives $\dot{\phi}$ in terms of ρ and p_ρ. Equation (A 6) can then be used to relate ρ and p_ρ for given values of the integrals I and χ. Similarly an equation for $\dot{\rho}$ can be obtained. The variation of ϕ with ρ can then be found by integrating $\mathrm{d}\phi/\mathrm{d}\rho = \dot{\phi}/\dot{\rho}$. Although possible in principle this procedure becomes very complicated for general λ due to the appearance of the exponent $\lambda^2+\lambda^{-2}$ in (A 6). In general the results do not appear to be expressible in terms of known functions. For $\lambda = 1$, however, the constraint $\zeta_0 = 0$ reduces to a point symmetry (see §3c) and tractable formulae result. We shall give the details for this case.

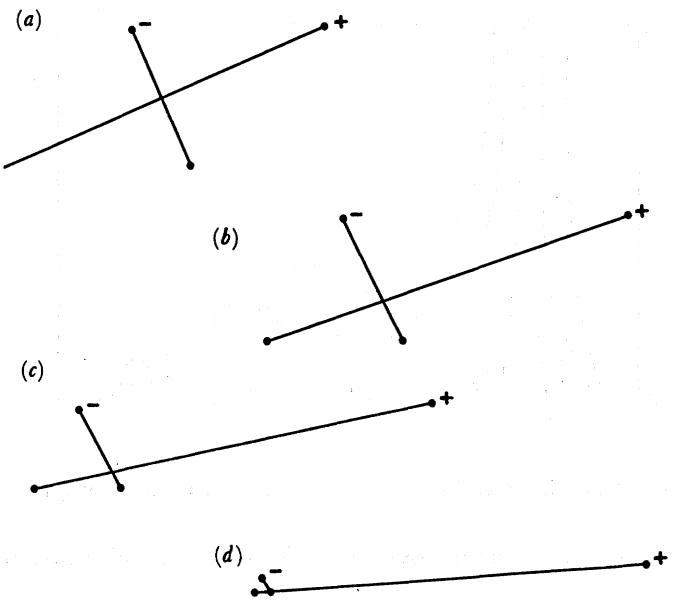

FIGURE A 3. Steady states of rotation for two pairs of vortices. The lines shown connect vortices of the same sign. The sign (+ or −) is shown at the location of vortices $z_1^{(\pm)}$. The smallest of Havelock's 'double alternate rings' (a rhombus) arises for $\lambda = 1$ (top). As λ decreases the steady state becomes a small (equilateral) triangle orbiting a distant, single vortex.

For $\lambda = 1$ (and for convenience we rescale length and time so that also $\Gamma = 1$), (3.20) reduces to

$$\dot{\zeta}_+^* = \frac{\mathrm{i}}{\pi} \frac{\zeta_+^2}{\zeta_-(\zeta_+^2 - \zeta_-^2)}, \tag{A 17a}$$

$$\dot{\zeta}_-^* = \frac{\mathrm{i}}{\pi} \frac{\zeta_-^2}{\zeta_+(\zeta_-^2 - \zeta_+^2)}. \tag{A 17b}$$

Substituting (A 3) into the second of these and resolving real and imaginary parts of both sides we get

$$\frac{\mathrm{d}\phi}{\mathrm{d}\rho} = \frac{\dot{\phi}}{\dot{\rho}} = \frac{I}{\rho^2 p_\rho} \frac{\rho^4 - I^2 + 3(\rho p_\rho)^2}{\rho^4 - 3I^2 + (\rho p_\rho)^2} \tag{A 18}$$

or in terms of the variables r, p introduced in (A 9)

$$\frac{\mathrm{d}\phi}{\mathrm{d}r} = \frac{I}{2\rho} \frac{\mathrm{d}\phi}{\mathrm{d}\rho} = \frac{I^2}{2\rho^3 p_\rho} \frac{r^2 - 1 + 3rp}{r^2 - 3 + rp}$$

$$= \pm \frac{1}{2r\sqrt{(rp)}} \frac{r^2 - 1 + 3rp}{r^2 - 3 + rp}, \tag{A 19}$$

where the overall sign is given by the signs of I and p_ρ.

Here r and p are related via (A 10), i.e. for this case by

$$r^2(1+rp)^2 = \chi\{(1 - rp - r^2)^2 + 4rp\}. \tag{A 20}$$

We solve this quadratic for rp in the form

$$1 + rp = (r^2\chi \pm Q)/(r^2 - \chi), \tag{A 21a}$$

where

$$Q = \sqrt{\{r^2\chi[(r^2-4)(r^2-\chi) + r^2\chi]\}} = r\sqrt{\{\chi[(r^2-2)^2 - 4(1-\chi)]\}}. \tag{A 21b}$$

In figure A 1 we have labelled the level curves shown as π, ρ, σ, τ and ω. For π and ρ we have $(0<)\,\chi<1$, $\chi>1$ for τ and ω, and σ is the separatrix $\chi=1$. The upper branches of ω and τ arise from (A 21 *a*) with the plus sign, the lower branches with the minus sign. Along π and ρ the sign to be used in (A 21 *a*) changes as described below. The signs to be used for the different parts of the separatrix σ are shown in the figure. The saddle point is at $(r,p)=(\sqrt{2},\frac{1}{2}\sqrt{2})$, and the separatrix has the asymptotes $r=1$ and $p=1$, and intersects the r-axis at $(\sqrt{5}\pm1)/2$.

For $\chi>1$ we always get two branches. The positive sign in (A 21 *a*) gives the upper branch corresponding to exchange scattering. The negative sign in (A 21 *a*) gives the 'bubble' corresponding to bound motion. This 'bubble' meets the r-axis at two points $r=r_\pm$ where

$$r_\pm=\{\sqrt{1+4\chi})\pm1\}/2\sqrt{\chi}. \tag{A 22}$$

Note that the topology shown in figure A 1 is corroborated by simple results such as

$$\{\sqrt{(1+4\chi)}-1\}/2\sqrt{\chi}\geqslant\tfrac{1}{2}(\sqrt{5}-1)\Leftrightarrow\chi(\chi-1)\geqslant0. \tag{A 23}$$

For $0<\chi<1$ we again get two branches both corresponding to direct scattering. The sign to be used in (A 21 *a*) changes along these branches. The changes in sign occur at the positions of the zeros of Q, namely

$$r^2=q_\pm\equiv2(1\pm\sqrt{(1-\chi)}). \tag{A 24}$$

For the small-r segment, used for calculating direct scattering below, we note that $\chi<q_-$.

Consider now starting off two vortex pairs from an initial configuration of the type described by (4.3) and shown in figure 1. An easy calculation gives the values of ρ and p_ρ as (recall $\lambda\delta=1$ for the integrable case)

$$\rho=D,\quad\text{and}\quad p_\rho=2DR\sin\theta,\quad\phi=\gamma. \tag{A 25 *a–c*}$$

Thus, (cf. (4.6) and (4.8))

$$r=1/2R\cos\theta=2/\hat{I} \tag{A 25 *d*}$$

$$p=2R\sin^2\theta/\cos\theta=4R^2\sin^2\theta/\hat{I}. \tag{A 25 *e*}$$

For fixed $\theta(\neq0)$ we thus start out in the phase diagram of figure A 1 at a large value of p and finite r.

Substituting (A 21 *a*) into (A 19) we get after some simple algebra

$$\frac{\mathrm{d}\phi}{\mathrm{d}r^2}=\frac{1}{4r^2}\left(\frac{r^2-\chi}{r^2(\chi-1)+\chi\pm Q}\right)^{\frac{1}{2}}\left(1\pm\frac{2r^2\chi}{Q}\right). \tag{A 26}$$

(The overall sign has been omitted here so as not to confuse it with the $\pm$ in front of Q. The latter leads to various branches in the (r,p) diagram as explained above.) To evaluate the change in ϕ for exchange scattering we must integrate (A 26) from $r^2=\chi$ to ∞. Thus

$$(\delta\phi)_{\text{exchange}}=\int_\chi^\infty\frac{1}{4r^2}\left(\frac{r^2-\chi}{r^2(\chi-1)+\chi+Q}\right)^{\frac{1}{2}}\left(1+\frac{2r^2\chi}{Q}\right)\mathrm{d}r^2. \tag{A 27}$$

For direct scattering we must first integrate (A 26) with the plus sign from $r^2 = \chi$ to $r^2 = q_-$ (see (A 24)). Then we must integrate (A 26) with the minus sign from $r^2 = q_-$ to $r^2 = r_-^2$ (see (A 22)). By symmetry the total change in ϕ is twice these integrals. Thus,

$$(\delta\phi)_{\text{direct}} = 2\int_{r_-^2}^{q_-} \frac{1}{4r^2}\left(\frac{r^2-\chi}{r^2(\chi-1)+\chi-Q}\right)^{\frac{1}{2}}\left(1-\frac{2r^2\chi}{Q}\right)\mathrm{d}r^2 - 2\int_{\chi}^{q_-} \frac{1}{4r^2}\left(\frac{r^2-\chi}{r^2(\chi-1)+\chi+Q}\right)^{\frac{1}{2}}\left(1+\frac{2r^2\chi}{Q}\right)\mathrm{d}r^2. \quad \text{(A 28)}$$

The integrals (A 27), (A 28) were evaluated numerically. In so doing it was occasionally useful to eliminate certain singularities of the integrands at the limits of integration. For such transcriptions the identity

$$Q^2-\{r^2(\chi-1)+\chi\}^2 = \chi(r^2-\chi)\,(r^2-r_-^2)\,(r^2-r_+^2) \quad \text{(A 29)}$$

is useful. Figure 2 and table 1, described previously in §4*a*, show the results. For direct scattering (A 27) gives the scattering angle directly. For exchange scattering (A 28) differs from the scattering angle by $\frac{1}{2}\pi$ as described in §4*a*. In the limit $R\to\infty$ the parameter χ and the parameter $\hat{I}$ introduced in (4.8) are related by

$$\chi = 4/\hat{I}^2. \quad \text{(A 30)}$$

An analytical expression for the scattering time (cf. figure 3) can be derived similarly.

Appendix B. Coaxial pairs

The hamiltonian is given by (3.14) where by (3.10)

$$\zeta_0 = \mathrm{i}\Gamma(\lambda y_1+\lambda^{-1}y_2), \quad \text{(B 1}a\text{)}$$

$$\hat{\zeta}_0 = x_1+x_2, \quad \text{(B 1}b\text{)}$$

$$\zeta_+ = x_1-x_2, \quad \text{(B 1}c\text{)}$$

$$\zeta_- = \mathrm{i}\Gamma(\lambda y_1-\lambda^{-1}y_2). \quad \text{(B 1}d\text{)}$$

We have used the notation $x_1 \equiv x_1^{(+)} = x_1^{(-)}, x_2 \equiv x_2^{(+)} = x_2^{(-)}, y_1 \equiv y_1^{(+)} = -y_1^{(-)}, y_2 \equiv y_2^{(+)} = -y_2^{(-)}$. We shall always assume $y_1 > 0$. For pairs propagating in opposite directions we then have $y_2 < 0$. We refer to this case as opposite polarity. For pairs propagating in the same direction $y_2 > 0$. We refer to this case as same polarity.

Conservation of the hamiltonian gives the relation

$$|\zeta_0+\zeta_-|^{\lambda^2}|\zeta_0-\zeta_-|^{\lambda^{-2}}\frac{|\zeta_+^2-(\alpha_+\zeta_0+\alpha_-\zeta_-)^2|}{|\zeta_+^2-(\alpha_-\zeta_0+\alpha_+\zeta_-)^2|} = \sqrt{\hbar} \quad \text{(B 2)}$$

where $\hbar$ is given by (A 7). For $\zeta_0 \neq 0$ we now set

$$\zeta_- = \zeta_0\eta, \quad \zeta_+ = \mathrm{i}\zeta_0\xi. \quad \text{(B 3}a,b\text{)}$$

Then ξ, η are real and (B 2) becomes

$$|1+\eta|^{\lambda^2}|1-\eta|^{\lambda^{-2}}\frac{\xi^2+(\alpha_+ +\alpha_-\eta)^2}{\xi^2+(\alpha_- +\alpha_+\eta)^2}=\chi, \tag{B 4}$$

where

$$\chi=\sqrt{\hbar}/|\zeta_0|^{\lambda^2+\lambda^{-2}}. \tag{B 5}$$

(This is not the same quantity for which we used the symbol χ in Appendix A. However, it plays an analogous role, and so the nomenclature has been retained.) We note that

$$\eta=\frac{\lambda y_1-\lambda^{-1}y_2}{\lambda y_1+\lambda^{-1}y_2} \tag{B 6}$$

so $-1<\eta<1$ for same polarity and $|\eta|>1$ for opposite polarity.

Consider again the simple case $\lambda=1$ (and $\Gamma=1$) for which (B 4) simplifies to

$$|1-\eta^2|\,(\xi^2+1)=\chi(\xi^2+\eta^2) \tag{B 7a}$$

or, resolving the absolute value sign for the two cases

same polarity:
$$(\xi^2+\chi+1)\,(\eta^2+\chi-1)=\chi^2; \tag{B 7b}$$

opposite polarity:
$$(\xi^2-\chi+1)\,(\eta^2-\chi-1)=\chi^2. \tag{B 7c}$$

These equations represent hyperbolae in a (ξ^2,η^2) 'phase plane'.

Figure B 1 shows the construction of the hyperbolae (B 7) for the three different cases $0<\chi<1$ (panels (*a*), (*d*), left column), $\chi=1$ (panels (*b*), (*e*), middle column) and $\chi>1$ (panels (*c*), (*f*), right column). The top row is for same polarity, the bottom row for opposite polarity. We note that the lower branch of the hyperbola in panel (*f*) is never in the physically acceptable region $\xi>0, \eta>0$. In figure B 1 the 'physically accessible' part of a hyperbola, $\xi^2,\eta^2>0$, is shown in full, the physically inaccessible part is shown dashed.

The interpretation of these diagrams is straightforward from (B 1). Trajectories in which ξ can tend to infinity correspond to evolutionary paths in which the vortex pairs separate arbitrarily. Trajectories for which the vortex pairs can pass each other reach $\xi=0$. In figure B 2 we show trajectories of the vortices corresponding to the different cases identified in figure B 1. A case-by-case interpretation follows.

Opposite polarity

We can apparently always consider initial conditions in which x_2-x_1 is positive and large, so that the vortex pairs run up against each other. For $\chi>1$ (panel (*f*)) they never pass one another ($\xi>0$ always) but $|y_1-y_2|\to\infty$. An exchange scattering interaction has taken place as shown in figure B 2*f*, and new pairs 1^+2^- and 2^+1^- 'have formed' that depart symmetrically to $y=\pm\infty$.

We note that the simplest case of this type, $\zeta_0=0$, is not covered by this analysis. In this case all four vortices describe geometrically similar paths and the motion corresponds to that of a single vortex impinging on a 90° solid corner. It is a classical result (Bassett 1888; Lamb 1932), easily seen from (B 2), that the trajectories then are so-called Cotes's spirals, namely

$$x^{-2}+y^{-2}=\text{const.} \tag{B 8}$$

PHILOSOPHICAL TRANSACTIONS OF THE ROYAL SOCIETY A MATHEMATICAL, PHYSICAL & ENGINEERING SCIENCES

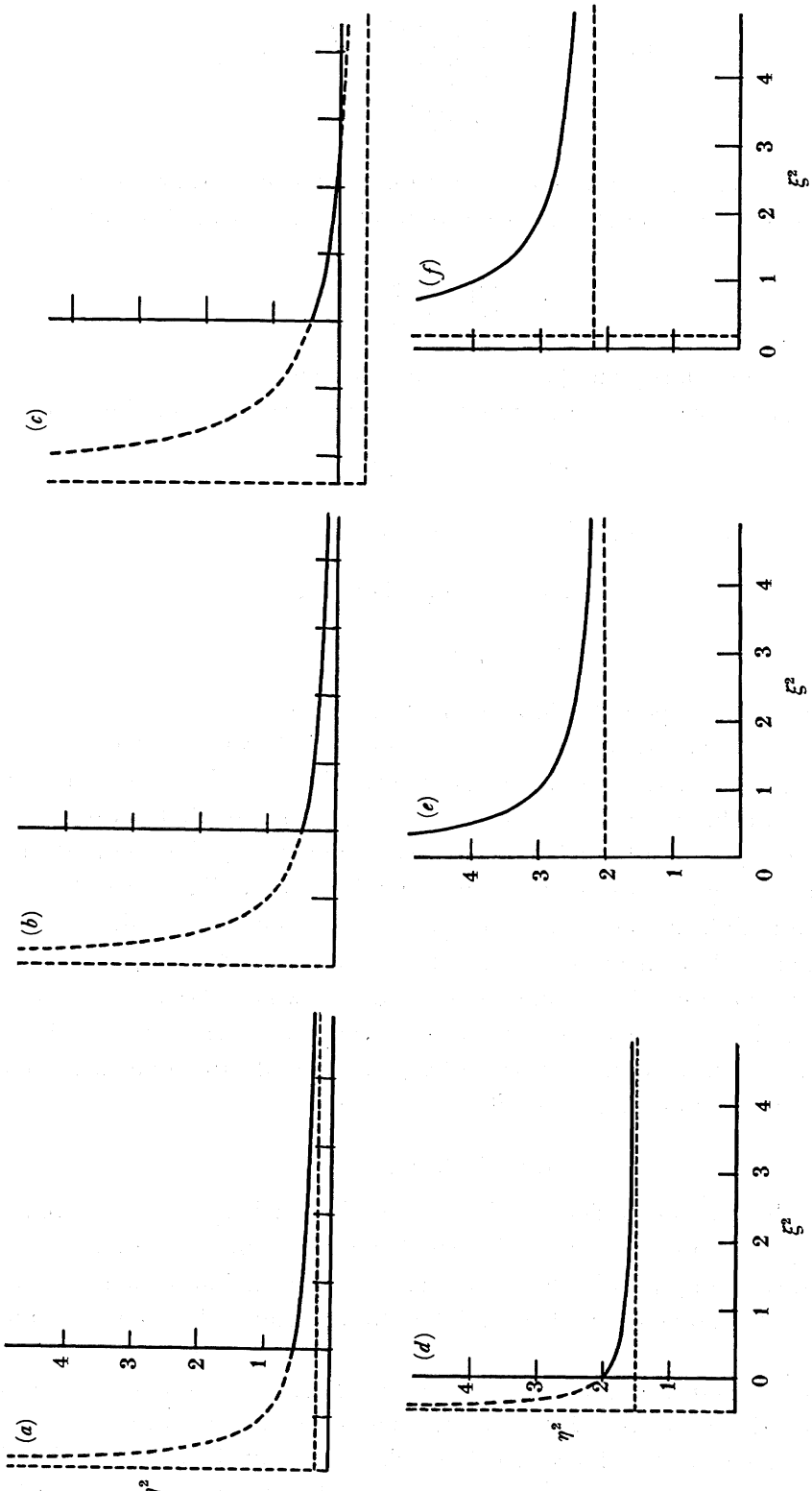

FIGURE B 1. 'Phase plane' trajectories for coaxial pairs with $\lambda = 1$. All trajectories are hyperbolae. The physically accessible parts are shown in full, physically inaccessible parts are shown dashed. The coordinates ξ^2 and η^2 are defined in Appendix B. The top row, (*a*)–(*c*), is for the case of 'same polarity'. The bottom row, (*d*)–(*f*), is for 'opposite polarity'. (*a*) $\chi < \chi_e = 1$; (*b*) $\chi = \chi_e$; (*c*) $\chi > \chi_e$. The interpretation of these curves is given in Appendix B.

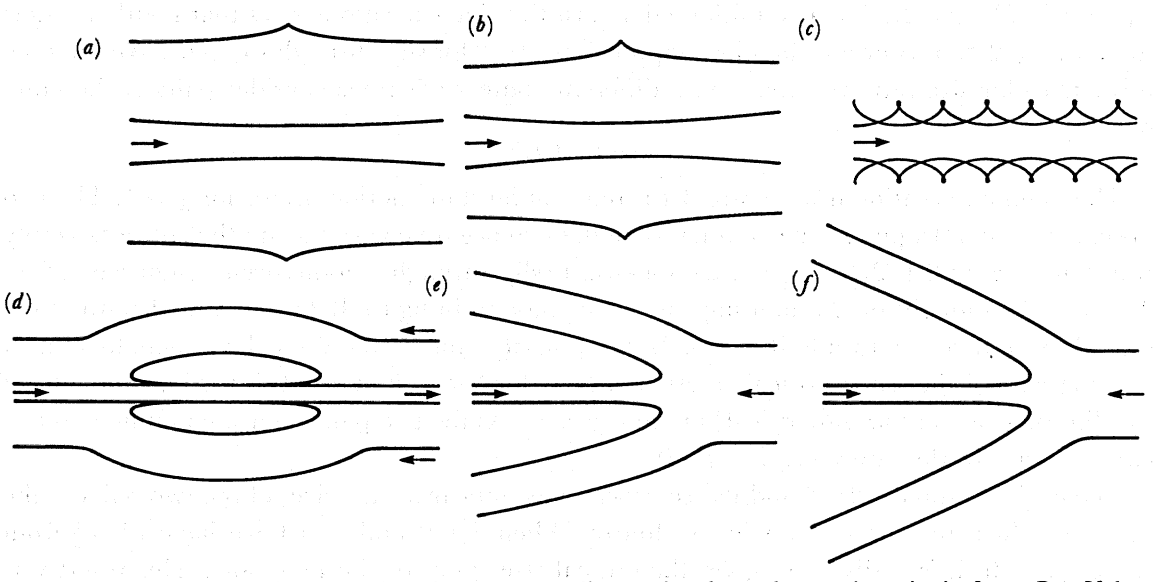

FIGURE B 2. Real space trajectories of vortices corresponding to the phase plane trajectories in figure B 1. Values of χ do not correspond exactly but were chosen to bring out qualitative features of the motion with greatest clarity. (*a*)–(*c*) These trajectories are for 'same polarity': (*a*) the 'slip-through' mode; (*b*) crossover to (*c*) 'leapfrog' motion. (*d*)–(*f*) These trajectories are for 'opposite polarity': the retrograde loops of the direct scattering (*d*) become longer and longer as the critical condition (*e*) is approached; (*f*) exchange interaction.

The size of the 'newly formed' pairs is given by conservation of the hamiltonian. If $y_1^{(0)}, y_2^{(0)}$ are the initial values of y_1, y_2 at large initial separation of the two original pairs, and d is the size of the new pairs (by symmetry the two pairs have the same size), then

$$d^2 = 2y_1^{(0)}(-2y_2^{(0)}) = \sqrt{h}. \tag{B 9}$$

The angle θ at which the two new pairs depart (see figure B 2*f*) is given by conservation of momentum

$$d\cos\theta = y_1^{(0)} + y_2^{(0)} = |\zeta_0|. \tag{B 10}$$

Thus

$$\cos^2\theta = \chi^{-1}. \tag{B 11}$$

For $0 < \chi < 1$ we have a direct scattering as shown in figure B 2*d*. When $x_1 = x_2$, i.e. $\xi = 0$, we have from (B 7*c*) that $\eta^2 = (1-\chi)^{-1}$ or from (B 6)

$$y_2/y_1 = -\{\sqrt{(1-\chi)} \pm 1\}^2/\chi \tag{B 12}$$

(these two values are reciprocals). The retrograde loop that one pair negotiates changes with χ becoming infinitely long as $\chi \to 1$ (B 2*e*).

The critical value $\chi = 1$ (panel (*e*) in figures B 1, B 2) is right at the cross-over between exchange and direct scattering. Because $\xi \to 0$ asymptotically for $\chi = 1$ (figure B 1*e*), we see that the two pairs in this case tend to collinearity at infinite separation. Thus, one pair is entirely 'back-reflected' as seen in figure B 2*e*. This corresponds with (B 11) where $\theta = 0, \pi$ for $\chi = 1$.

If we 'shoot' two vortex pairs towards each other from a great distance, we have $\eta^2 = \chi + 1$. If we insist that the pairs pass one through the other, we must have $\chi < 1$. Thus, we have a limiting value of $|\eta|$ equal to $\sqrt{2}$. According to (B 6) this translates into limiting ratios y_2/y_1

equal to $-(3\pm2\sqrt{2})$. The two initial pairs must thus have a ratio of sizes that is either larger than $3+2\sqrt{2}\approx5.83$ or less than its reciprocal $3-2\sqrt{2}$ for slip-through to occur. We shall see this particular size ratio re-emerge in a different context when we consider pairs of the same polarity.

Same polarity

The main observation from figure B 1 is that bound state motion occurs for $\chi>1$. The two positive vortices 'leapfrog' one another as do the two negative vortices and the entire assembly translates (figure B 1, 2*c*). At $\chi=1$ a cross-over to slip-through motions occurs (figure B 1, 2*b*). This may be thought of as a limiting case of the motion in figure B 2*c* where the length of the spatial cycle diverges to infinity. (For 'same polarity' the cross-over is best thought of as a limiting case of the 'supercritical' motion, $\chi>1$; for 'opposite polarity' it is best thought of as a limiting case of the 'subcritical' motion, $\chi<1$.) As the two pairs separate infinitely in this case they attain the same size, i.e. $\eta\to0$.

The critical ratio $3+2\sqrt{2}$ and its reciprocal now appear for the sizes of the two pairs at the moment when all four vortices are collinear. When $\xi=0$ and $\chi=1$ we have $\eta^2=\frac{1}{2}$ from (B 7*b*), which, it is easily seen, gives the critical size ratio for the two pairs. This result was discovered by Gröbli (1877) and later by Love (1894). When the size ratio at collinearity is smaller than $3-2\sqrt{2}$ or greater than $3+2\sqrt{2}$ the pairs separate arbitrarily with time.

There is an analogy between the behaviour of vortex pairs colliding and then passing one another and the interaction of solitons in certain one-dimensional PDEs. Indeed, because the state of the vortex pairs long after collision is identical to the state before, one can only detect the collision by the retardation in arrival at a given x-station of a given pair. This is the analogue of a phase shift for a travelling wave. Similarly the bound motions are analogues of 'breather' states in soliton-bearing systems. Analytical expressions for the retardation can be derived, however we shall not pause to do so here.

We now consider the case $\lambda\neq1$. Our first objective is to produce a 'phase plane' analysis analogous to that for $\lambda=1$ above. If we solve (B 4) for ξ^2 we get

$$\xi^2(\chi-|1+\eta|^{\lambda^2}|1-\eta|^{\lambda^{-2}})=(\alpha_++\alpha_-\eta)^2|1+\eta|^{\lambda^2}|1-\eta|^{\lambda^{-2}}-(\alpha_-+\alpha_+\eta)^2\chi. \tag{B 13}$$

We consider separately the two functions

$$f(\eta;\lambda)\equiv|1+\eta|^{\lambda^2}|1-\eta|^{\lambda^{-2}} \tag{B 14a}$$

and

$$g(\eta;\lambda,\chi)\equiv(\alpha_++\alpha_-\eta)^2|1+\eta|^{\lambda^2}|1-\eta|^{\lambda^{-2}}-(\alpha_-+\alpha_+\eta)^2\chi. \tag{B 14b}$$

For f we have

$$f(-1;\lambda)=f(1;\lambda)=0,\quad f(0;\lambda)=1. \tag{B 15a,b}$$

Also, differentiating with respect to η it is easily seen that f has a unique (local) maximum at

$$\eta_0=(\lambda^2-\lambda^{-2})/(\lambda^2+\lambda^{-2})=-2\alpha_-\alpha_+/(\alpha_-^2+\alpha_+^2). \tag{B 15c}$$

The points $\eta=\pm1$, where $f=0$, are minima. The value of f at η_0 is

$$\chi_c=\frac{2^{\lambda^2+\lambda^{-2}}}{(\lambda^4+1)^{\lambda^{-2}}(\lambda^{-4}+1)^{\lambda^2}}. \tag{B 15d}$$

Note that $\lambda^2+\lambda^{-2}>2$ for $\lambda\neq1$ and that $\chi_c=1$ for $\lambda=1$. A diagram of $f(\eta;\lambda)$ for $\lambda^2=0.9$ is shown in figure B 3. For given χ in (B 13) we now see that the coefficient of ξ^2 will have four

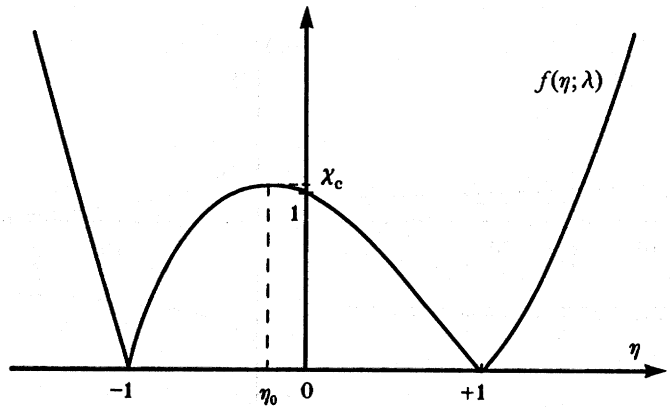

FIGURE B 3. Plot of the function $f(\eta;\lambda)$ for $\lambda<1$. The local maximum at η_0 and the corresponding value χ_c are shown.

zeros for $0<\chi<\chi_c$ (two within $-1<\eta<1$, one in either of $\eta<-1$ and $\eta>1$), three zeros for $\chi=\chi_c$ (one at $\eta=\eta_0$, one in either of $\eta<-1$ and $\eta>1$), and just two zeros for $\chi>\chi_c$ (one in either of $\eta<-1$ and $\eta>1$).

We next turn to $g(\eta;\lambda,\chi)$. For (B 13) to have physically acceptable solutions for ξ^2 it is clearly necessary that g and $\chi-f$ have the same sign. We may write g as

$$g(\eta;\lambda,\chi)=\tfrac{1}{2}\{(\alpha_+ +\alpha_-\eta)^2+(\alpha_- +\alpha_+\eta)^2\}(f-\chi)+(1-\eta^2)(f+\chi)/2\Gamma^2. \qquad \text{(B 16}a\text{)}$$

Thus, $g>0$ for $|\eta|<1$ and $f>\chi$, and $g<0$ for $|\eta|>1$ and $f<\chi$. In these intervals there is no physically acceptable solution for ξ^2.

For $f=\chi$

$$g(\eta;\lambda,\chi)=(1-\eta^2)\chi/\Gamma^2. \qquad \text{(B 16}b\text{)}$$

These values of g are positive (negative) for $|\eta|<1(|\eta|>1)$. Further points of reference are that

$$g(\pm1;\lambda,\chi)=-(\alpha_-\pm\alpha_+)^2\chi<0, \qquad \text{(B 16}c\text{)}$$

$$g(-\alpha_+/\alpha_-;\lambda,\chi)<0, \qquad \text{(B 16}d\text{)}$$

$$g(-\alpha_-/\alpha_+;\lambda,\chi)>0. \qquad \text{(B 16}e\text{)}$$

The analysis for same polarity is quite analogous to the special case $\lambda=1$ discussed above. For $\chi>\chi_c$ there are two zeros of g in the interval $-1<\eta<1$ and g is positive between the two zeros and negative beyond either. Because $\chi-f$ is always positive there are solutions for ξ^2 in the interval between the two roots of g and ξ^2 is bounded. Thus, we have a régime of bounded motion. For $\chi=\chi_c$ we see from (B 13) that $\xi^2\to\infty$ when $\eta\to\eta_0\pm$. It may also be seen that one of the zeros of g will be between η_0 and 1, the other between -1 and η_0. Finally for $0<\chi<\chi_c$ there will be two solutions of $f=\chi$ in $-1<\eta<1$. Call these η_a and η_b, where $\eta_a<\eta_b$. We can then show that g has one zero in the interval $-1<\eta<\eta_a$ and one in $\eta_b<\eta<1$. Hence, there are no physically acceptable solutions ξ^2 for $\eta_a<\eta<\eta_b$ and $\xi^2\to\infty$ for $\eta\to\eta_a-$ and for $\eta\to\eta_b+$.

The ξ^2 against η 'phase portraits' for same polarity are shown in figure B 4. For $\lambda=1$ the diagrams are symmetrical about the ξ^2-axis, and reduce to figure B 1. The interpretation of figure B 4 is quite similar to that of figure B 1 with bound-state motion for $\chi>\chi_c$ (figure B 4c) and slip-through for $0<\chi<\chi_c$ (figure B 4a). At the cross-over $\chi=\chi_c$ (figure B 4b) both

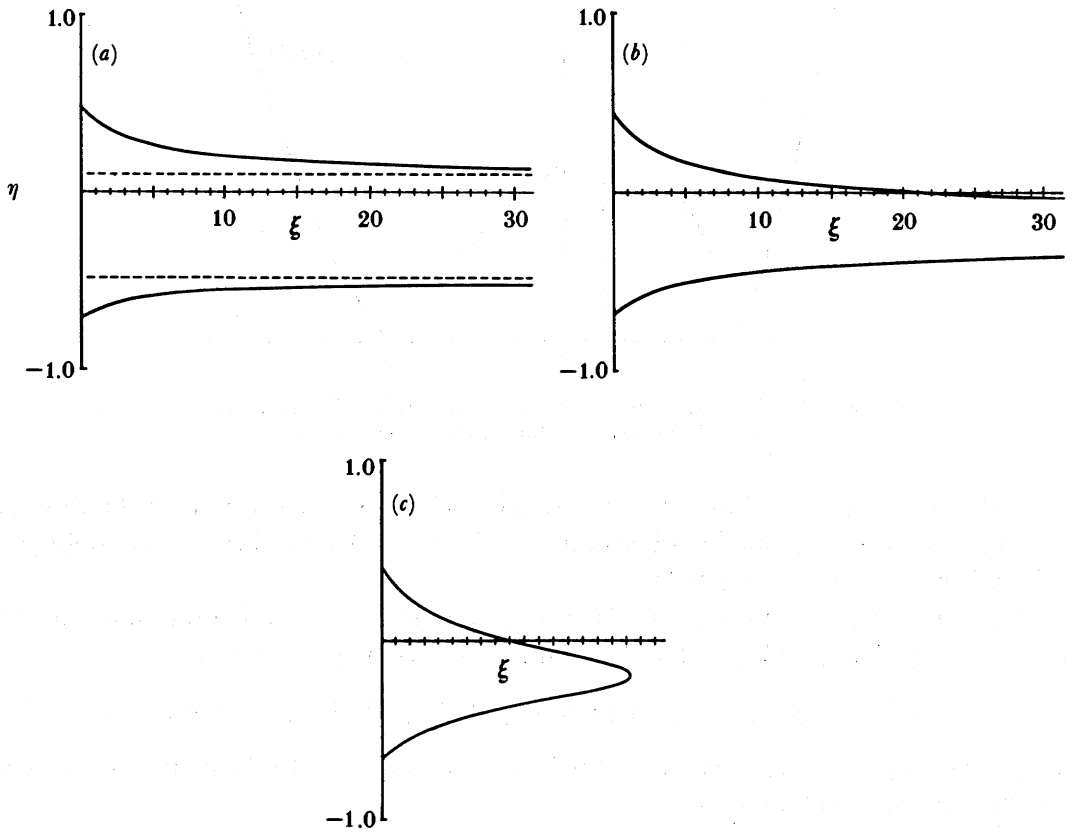

FIGURE B 4. 'Phase plane' diagrams for 'same polarity' and $\lambda < 1$. These figures correspond to (*a*)–(*c*) in figure B 1. (*a*) $\chi < \chi_c$; (*b*) $\chi = \chi_c$; (*c*) $\chi > \chi_c$.

branches asymptote to η_0. From (B 15*c*) it is easy to see that the ratio of sizes as the pairs separate infinitely in this case is λ^{-2}.

The critical size ratios for slip-through when all vortices are collinear are given by the zeros of $g(\eta; \lambda, \chi_c)$. For $\lambda \neq 1$ these two zeros are not reciprocals. For $\lambda = 1$ relabelling the vortices by interchanging indices 1 and 2 is equivalent to the symmetry $\xi \to -\xi, \eta \to -\eta$. For $\lambda \neq 1$ this relabelling must be accompanied by the change $\lambda \to \lambda^{-1}$. Thus, the zeros of g and indeed the entire trajectories in figure B 4 for positive and negative η are not symmetrical about the ξ^2 axis.

In figure B 5 we show the result of a numerical determination of the critical size ratio at collinearity as a function of λ. We show just one branch. If we call the function shown in figure B 5 $r(\lambda)$, the other branch (not shown) is $r^{-1}(\lambda^{-1})$. The graph passes through $\lambda = 1$, $r = 3+2\sqrt{2}$. The size ratio $r(\lambda)$ has a limiting value as $\lambda \to \infty$. The physical interpretation of this result is straightforward if one recalls the streamline pattern for a pair of vortices in a frame of reference moving uniformly along with them (figure B 6). In this frame the flow is steady and pathlines of passively advected particles coincide with streamlines. There is a trapped region of fluid inside the oval dividing streamline. A sufficiently weak second 'vortex pair' inside this region will simply be advected by the stronger pair with no possibility of escape. The points A, A′ are right at the crossover from bound to unbound motion in the limit where one pair is

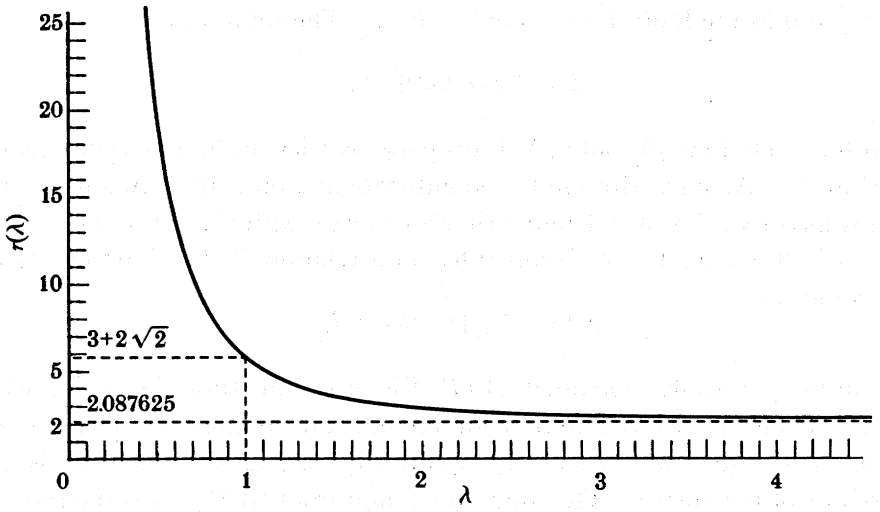

FIGURE B 5. The critical size ratio at collinearity for coaxial vortex pairs as a function of λ. This function has two branches, $r(\lambda)$ shown here and $r^{-1}(\lambda^{-1})$. The ratio passes through $3+2\sqrt{2}$ for $\lambda = 1$ and asymptotes to a value $\delta \approx 2.0872538\ldots$ given by (B 17) as $\lambda \to \infty$.

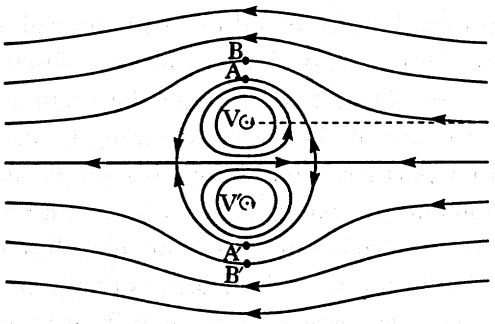

FIGURE B 6. The streamline pattern of a translating vortex pair in its rest frame of reference. The limiting value of r as $\lambda \to \infty$ in figure B 5 is given by the ratio AA′/VV′. Acton (1976) incorrectly determined this value as the ratio BB′/VV′.

infinitely weaker than the other. The size ratio $\delta = \mathrm{AA}'/\mathrm{VV}'$ is given by elementary considerations as the non-trivial solution of

$$e^{\delta} = (\delta+1)^2/(\delta-1)^2. \tag{B 17}$$

To derive this relation from our earlier analysis we let

$$\eta = (1-y_2/\lambda^2 y_1)/(1+y_2/\lambda^2 y_1) = 1-2\delta\lambda^{-2} \tag{B 18}$$

to leading order in λ^{-2} where $\delta \equiv y_2/y_1$ is the size ratio. As $\lambda \to \infty$ we can expand the constituents of $g(\eta; \lambda, \chi_c)$ as follows:

$$(\alpha_+ + \alpha_- \eta)^2 = \lambda^{-2}(1+\delta)^2/\Gamma^2 + O(\lambda^{-4}), \tag{B 19a}$$

$$(\alpha_- + \alpha_+ \eta)^2 = \lambda^{-2}(1-\delta)^2/\Gamma^2 + O(\lambda^{-4}), \tag{B 19b}$$

$$|1+\eta|^{\lambda^2}|-\eta|^{\lambda^{-2}} \sim 2^{\lambda^2}\exp(-\delta) \tag{B 19c}$$

and

$$\chi_c \sim 2^{\lambda^2}. \tag{B 19d}$$

Thus, $g(\eta;\lambda,\chi_c)=0$ in the limit $\lambda\to\infty$ implies (B 17). The solution is

$$\delta = 2.0872538\ldots. \tag{B 20}$$

We mention that Acton (1976; only §2 of this paper is relevant here) has discussed some of these points. However, Acton's criterion for bound-state motions, (6) of Acton (1976), differs from ours and is incorrect. For $\lambda=1$ both criteria coincide with the earlier criteria of Gröbli (1877) and Love (1894). As $\lambda\to\infty$ Acton is led to a relation ((14) of Acton 1976) that in our notation would be

$$e^{\delta-1} = (\delta+1)^2/(\delta-1)^2. \tag{B 21}$$

This differs from the physically motivated (B 17). Closer examination shows that what Acton has calculated (via an erroneous criterion for bound-state motion) is the position of that streamline, shown in figure B 6, which asymptotically (i.e. as $x\to\pm\infty$) levels off at the y-coordinate of one of the vortices. The solution δ found from (B 21) gives the ratio BB′/VV′ in figure B 6. The method used by Acton (1976) for determining when the vortices are locked in periodic bound motion for same polarity is in general inadequate.

The case of opposite polarity differs significantly from that outlined for $\lambda=1$ in at least two respects. First, when shot in from infinity two different pairs will always manage to pass one another, i.e. we always have direct scattering (as already discussed for cases without the symmetry of a common axis, see §4*a*). Even though the original pairs can break up upon approaching one another, because of the different strengths each vortex must eventually become paired with its initial partner. Combining this simple insight with the constraints imposed by energy and momentum conservation, we see that we can have more or less elaborate loops of non-neutral, intermediate pairs, but the ultimate outcome is certain: the original pairs re-emerge moving in the same directions as they were initially. Hence, the phase plane diagram now always has trajectories that come in from large values of ξ^2 and intersect the η-axis. An example is shown in figure B 7*a*. Second, it is now possible to have bound-state motion. This comes about in the 'phase plane', as indicated in figure B 7, by a 'pinch off' of the loop in figure B 7*a* (see the portions of the phase trajectory by the arrows in figure B 7*a*, *b*).

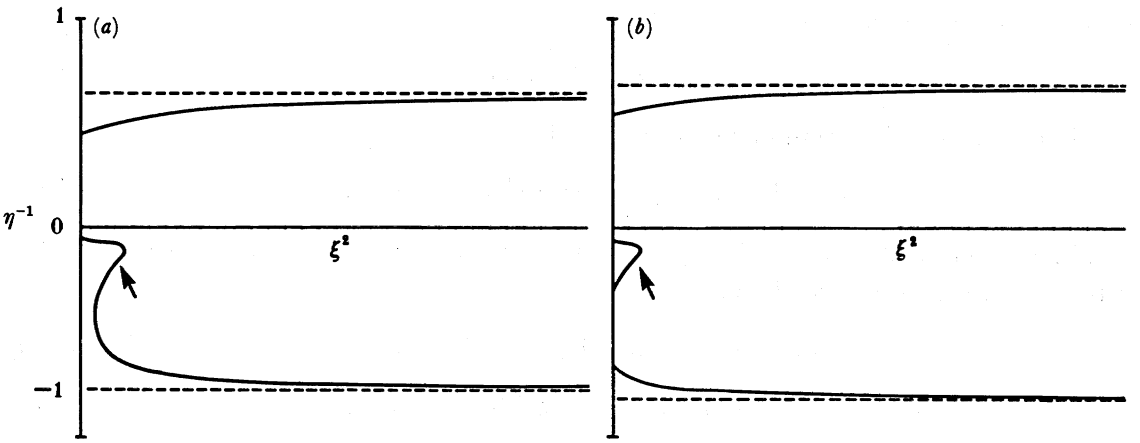

FIGURE B 7. The case of 'opposite polarity' for $\lambda<1$ can lead to a régime of bound motion (*b*) for sufficiently large values of χ. In (*a*) there is retrograde motion (arrow) but no bound régime. In (*b*) the possibility of bound motion is clearly indicated (arrow).

Bound motion of two pairs with a common axis in the opposite polarity case is easily understood if the motion is viewed as that of two vortices of opposite sign but different strengths close to a plane wall. A weaker negative vortex can orbit a stronger positive vortex while the two of them move along the wall. An example of real space trajectories for this type of motion is shown in figure B 8. The trajectories of one pair of vortices is shown by the plain lines, the other pair by the bold lines. The small arrows indicate the direction of motion.

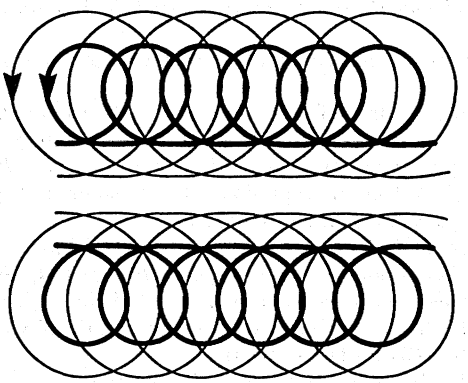

FIGURE B 8. Vortex trajectories corresponding to the bound motion régime identified in figure B 7*b*. The vortices tracing the bold trajectories have opposite circulations as do the vortices providing the other two tracks. Arrows indicate direction of motion, and the entire plot has a horizontal axis of symmetry.

The determination of this régime of bounded motion can be approached by investigating the conditions under which both ξ^2 and $\mathrm{d}\xi^2/\mathrm{d}\eta$ vanish for some η. By (B 13) this reduces to an inquiry of when g and $\mathrm{d}g/\mathrm{d}\eta$ both vanish, and this in turn yields a cubic equation for η. However, we shall not elaborate on the details here.

REFERENCES

Acton, E. 1976 The modelling of large eddies in a two-dimensional shear layer. *J. Fluid Mech.* **76**, 561–592.

Agmon, N. 1984 Fine structure in the dependence of final conditions on initial conditions in the classical collinear H_2+H dynamics. *J. chem. Phys.* **76**, 1309–1316.

Aref, H. 1979 Motion of three vortices. *Phys. Fluids* **22**, 393–400.

Aref, H. 1982 Point vortex motions with a center of symmetry. *Phys. Fluids* **25**, 2183–2187.

Aref, H. 1983 Integrable, chaotic, and turbulent vortex motion in two-dimensional flows. *A. Rev. Fluid Mech.* **25**, 345–389.

Aref, H. 1985 Chaos in the dynamics of a few vortices – fundamentals and applications. In *Theoretical and applied mechanics* (ed. F. I. Niordson & N. Olhoff), pp. 43–68. Amsterdam: Elsevier.

Aref, H. & Pomphrey, N. 1982 Integrable and chaotic motions of four vortices. I. The case of identical vortices. *Proc. R. Soc. Lond.* A **380**, 359–387.

Aref, H. & Siggia, E. D. 1981 Evolution and breakdown of a vortex street in two dimensions. *J. Fluid Mech.* **109**, 435–463.

Aref, H., Gharib, M. & Van Atta, C. W. 1987 Chaos in shear flows. AIAA paper 87-1251.

Aref, H., Kadtke, J. B., Zawadzki, I., Campbell, L. J. & Eckhardt, B. 1988 Point vortex dynamics: Recent results and open problems. *Fluid Dyn. Res.* (In the press.)

Bassett, A. B. 1888 *A treatise on hydrodynamics*. Deighton, Bell & Co. Vol. 2, p. 47. (Republished by New York: Dover Publ. (1961).)

Batchelor, G. K. 1967 *An introduction to fluid dynamics*. Cambridge University Press.

Campbell, D. K., Peyrard, M. & Sodano, P. 1986 Kink-antikink interactions in the double Sine–Gordon equation. *Physica* D **19**, 165–205.

Couder, Y. & Basdevant, C. 1986 Experimental and numerical study of vortex couples in two-dimensional flows. *J. Fluid Mech.* **173**, 225–251.

PHILOSOPHICAL TRANSACTIONS OF THE ROYAL SOCIETY A MATHEMATICAL, PHYSICAL & ENGINEERING SCIENCES

Domm, U. 1956 Über die Wirbelstrassen von geringster Instabilität. *Z. angew. Math. Mech.* **36**, 367–371.
Eckhardt, B. 1987 Fractal properties of scattering singularities. *J. Phys.* A. **20**, 5971–5979.
Eckhardt, B. 1988*a* Irregular scattering of vortex pairs. *Europhys. Lett.* **5**, 107–111.
Eckhardt, B. 1988*b* Integrable four-vortex motion. *Physics Fluids*. (In the press.)
Eckhardt, B. & Jung, C. 1986 Regular and irregular potential scattering. *J. Phys.* A **19**, L829–L833.
Friedrichs, K. O. 1966 *Special topics in fluid dynamics*. New York: Gordon & Breach.
Gottdiener, L. 1975 The multiple-collision region in non-reactive atom–diatom collisions. *Molec. Phys.* **29**, 1585–1595.
Greenhill, A. G. 1878 Plane vortex motion. *Q. Jl Math.* **15**, 10–29.
Gröbli, W. 1877 *Specielle Probleme über die Bewegung geradliniger paralleler Wirbelfäden* (86 pages). Zurich: Zürcher & Furrer.
Havelock, T. H. 1931 The stability of motion of rectilinear vortices in ring formation. *Phil. Mag.* (7) **11**, 617–633.
Hicks, W. M. 1922 On the mutual threading of vortex rings. *Proc. R. Soc. Lond.* A **102**, 111–131.
Hogg, N. G. & Stommel, H. M. 1985*a* The heton, an elementary interaction between discrete baroclinic geostrophic vortices and its implications concerning eddy heat-flow. *Proc. R. Soc. Lond.* A **397**, 1–20.
Hogg, N. G. & Stommel, H. M. 1985*b* Hetonic explosions: The breakup and spread of warm pools as explained by baroclinic point vortices. *J. atmos. Sci.* **42**, 1465–1476.
Jung, C. 1986 Poincaré map for scattering states. *J. Phys.* A **19**, 1345–1353.
Khanin, K. M. 1982 Quasi-periodic motions of vortex systems. *Physica* D **4**, 261–269.
Kirchhoff, G. R. 1876 *Vorlesungen über Mathematische Physik*, vol. 1. Leipzig: Teubner.
Koiller, J., Pinto de Carvalho, S., Rodrigues da Silva, R. & Goncalves de Oliviera, L. C. 1985 On Aref's vortex motions with a symmetry center. *Physica* D **16**, 27–61.
Lamb, H. 1932 *Hydrodynamics*, 6th edn. New York: Dover Publications.
Love, A. E. H. 1894 On the motion of vortices with a common axis. *Proc. Lond. math. Soc.* **25**, 185–194.
Manakov, S. V. & Shchur, L. N. 1983 Stochastic aspect of two-particle scattering. *Soviet Phys. JETP Lett.* **37**, 54–57.
McWilliams, J. C. 1984 The emergence of isolated coherent vortices in turbulent flow. *J. Fluid Mech.* **146**, 21–43.
McWilliams, J. C. & Zabusky, N. J. 1982 Interactions of isolated vortices. *Geophys. Astrophys. Fluid Dyn.* **19**, 207–227.
Moser, J. 1973 *Stable and random motions in dynamical systems* (198 pages). Princeton University Press.
Noid, D. W., Gray, S. K. & Rice, S. A. 1986 Fractal behavior in classical collisional energy transfer. *J. chem. Phys.* **84**, 2649–2652.
Novikov, E. A. 1975 Dynamics and statistics of a system of vortices. *Soviet Phys. JETP* **41**, 937–943.
Overman, E. A. & Zabusky, N. J. 1982 Coaxial scattering of Euler-equation translating V-states via contour dynamics. *J. Fluid Mech.* **125**, 187–202.
Petit, J-M. & Hénon, M. 1986 Satellite encounters. *Icarus* **66**, 536–555.
Press, W. H., Flannery, B. P., Teukolsky, S. A. & Vetterling, W. T. 1986 *Numerical recipes – the art of scientific programming* (818 pages). Cambridge University Press.
Rankin, C. C. & Miller, W. H. 1971 Classical S-matrix for linear reactive collisions of $H + Cl_2$. *J. chem. Phys.* **55**, 3150–3156.
Spirig, F. & Waldvogel, J. 1985 The three-body problem with two small masses: a singular-perturbation approach to the problem of Saturn's coorbiting satellites. In *Stability of the Solar System and its minor natural and artificial bodies* (*NATO Advanced Study Institute Series C*) (ed. V. Szebehely). Dordrecht: Reidel.
Synge, J. L. 1949 On the motion of three vortices. *Can. J. Math.* **1**, 257–270.
Tatsuno, M. & Honji, H. 1977 Two pairs of rectilinear vortices. *J. phys. Soc. Japan* **42**, 361–362.

PHILOSOPHICAL TRANSACTIONS OF THE ROYAL SOCIETY A MATHEMATICAL, PHYSICAL & ENGINEERING SCIENCES